8-2011

Modeling Instabilities of Electrically Driven Jets Under Constant or Variable Applied Field and Non-Zero Basic State Velocity

Sayantan Das
University of Texas-Pan American

MODELING INSTABILITIES OF ELECTRICALLY DRIVEN JETS UNDER CONSTANT OR VARIABLE APPLIED FIELD AND NON ZERO BASIC STATE VELOCITY

A Thesis
by
SAYANTAN DAS

Submitted to the Graduate School of the
University of Texas-Pan American
In partial fulfillment of the requirements for the degree of

MASTER OF SCIENCE

August 2011

Major Subject: Mathematics

MODELING INSTABILITIES OF ELECTRICALLY DRIVEN JETS UNDER CONSTANT OR VARIABLE APPLIED FIELD AND NON ZERO BASIC STATE VELOCITY

A Thesis
by
SAYANTAN DAS

COMMITTEE MEMBERS

Dr. Daniel N. Riahi
Chair of Committee

Dr. Dambaru Bhatta
Committee Member

Dr. Paul Bracken
Committee Member

Dr. Andras Balogh
Committee Member

August 2011

ABSTRACT

Das, Sayantan, Modeling Instabilities of Electrically Driven Jets under Constant or Variable Applied Field and Non Zero Basic State Velocity. Master of Science (MS), August, 2011, 52pp., 21 references, 5 titles.

We investigate the problem of instability of electrically forced axisymmetric jets with respect to temporally and spatially growing disturbances, within parameter regimes that affects the process of electrospinnning. Deriving a dispersion relation based on the relevant approximated versions of the equations of the electro-hydrodynamics for an electrically forced jet flow. For temporal instability, we find in the non-zero basic state velocity, the growth rate of the unstable mode is unaffected by the value of the basic state velocity. But, the basic state velocity affects the period of the unstable mode in the sense that it decreases the period, and the rate of increase of the frequency with respect to axial wave number increases with the basic state velocity. For spatial instability, we find that the growth rate of the unstable mode is dominated by the basic state velocity. The basic state velocity also affects the period of the unstable mode.

DEDICATION

This work is dedicated to my beloved parents (Satya Kr. Das,Ila Das) my sister Sanchaita Das,

& Brother Suman Bhattacharya

ACKNOWLEDGMENTS

First, I would like to thank my advisors, Dr. Daniel N. Riahi and Dr. Dambaru Bhatta, for enabling me to undertake these studies, for providing me with an interesting and challenging topic. Without their help and support this research would have been impossible. My thanks go to my thesis committee members: Dr. Paul Bracken, Dr. Andras Balogh for their suggestions.

TABLE OF CONTENTS

LIST OF FIGURES

Page

CHAPTER I

TEMPORAL INSTABILITY

The investigation of electrically forced jets is gaining importance in applications such as those to electro spraying, Baily (1981) and electro spinning, Hohman et al. (2001a-b). Electro spraying uses electric field to produce and control sprays of very small drops that are uniform in size. Electro spinning process uses electric fields to produce and control thin, uniform, high quality fibers. In the absence of electrical effects, it is observed that temporal growing disturbances can destabilize the free shear flows which include the jet flows. Several authors Hohman et al. (2001a), Drazin (1981), Fridrikh (2003), have done theoretical studies on temporal instability of the electrically forced jets in the presence of electrical effects. Hohman et al. (2001a) developed a theoretical understanding of temporal instabilities for an electrically forced jet with a static charge density. The equations for the dependent variables of the disturbances were based on the long wavelength and asymptotic approximations of the governing electro-hydrodynamic equations. They found that the dominance of the instabilities depends on the surface charge density and the radius of the jet. Saville (1971), studied interactions between electrical tractions at the interface of an electrically driven liquid jet and the linear temporal instability phenomena. It was found, in particular, that when viscous effects are small, sufficiently small strength of the electric fields tends to decrease the growth rate of a temporally

growing axisymmetric mode. However, when viscous effects predominate, then the only unstable disturbance is that due to the axisymmetric mode regardless of the magnitude of the field's strength. Other investigations of electrically driven jets with applications in electro spinning of nano fiber are reported in Yarin(2000), Sun et al.(2003), Li(2004), and Yu et al.(2004). Spatial instability of aixsymmetric electrically forced jets with variable applied field under idealistic conditions of zero or infinite electrical conductivity was studied analytically by Riahi (2009). He reported two spatial modes of instability each of which was enhanced with increasing the strength of the externally applied electric field.

1.1 Temporal Instability Case

In this present study, we follow an approach similar to that of Hohman et al. (2001a) to obtain a mathematical model for the electrically driven jets. We consider the problem of instability of electrically forced axisymmetric jets with respect to temporally growing disturbances. We derive a dispersion relation based on the relevant approximated versions of the equations of the electro-hydrodynamics for an electrically forced jet flow. The approximations include the assumptions that the length scale along the axial direction of the jet is much larger than that in the radial direction of the jet and the disturbances are axisymmetric and infinitesimal in amplitude. This work is an extension of Hohman et al. (2001a) in the sense that our model incorporates non-zero basic velocity and non-zero surface charge density. We then determine the dispersion relation, which relates the growth rate of the spatially growing disturbances to the wave number in the axial direction, the frequency and the non-dimensional parameters of the model. We found a number of interesting results. In particular, the growth rate of the temporally growing disturbances is found to be independent of the basic state velocity, while the frequency and equivalently the period of the growing disturbances found to depend notably on the basic

state velocity. It is also observed from numerical investigations that there are two modes of instability for small values of the wavenumber.

1.2 Mathematical Formulation

The present theoretical investigation for the mathematical modeling of the electrically driven jets is based on the original governing electro-hydrodynamic equations Melcher &G.I. Taylor (1969) for the mass conservation, momentum, charge conservation and the electric potential. The system is given by

$$\frac{D\rho}{Dt} + \rho\nabla.\vec{u} = 0 \tag{1a}$$

$$\rho\frac{D\vec{u}}{Dt} = -\nabla P + \nabla.\nabla\left(\mu\vec{u}\right) + q\vec{E} \tag{1b}$$

$$\frac{Dq}{Dt} + \nabla.\left(K\vec{E}\right) = 0 \tag{1c}$$

$$\vec{E} = -\nabla\Phi \tag{1d}$$

where $\frac{D}{Dt} = \frac{\partial}{\partial t} + \vec{u}.\nabla$ is the total derivative. Here $\vec{u}$ is the velocity vector, P is the pressure, $\vec{E}$ is the electric field vector, Φ is the electric potential, q is the free charge density, ρ is the fluid density, μ is the dynamic viscosity, K is electric conductivity and t is the time variable. The geometry we use is shown in figure 1.

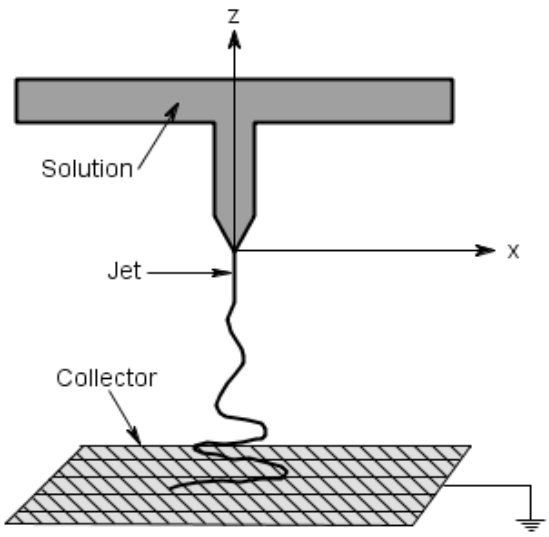

Figure 1. Electrospinning model

The internal pressure in the jet can be found by taking into consideration the balances across the free boundary of the jet between the pressure, viscous forces, capillary forces and the electric energy density plus the radial self-repulsion of the free charges on the free boundary G.I Taylor (1969). Assuming the ambient air to be motionless and passive, this yield the following expression for the pressure P in the jet

$$P = \gamma\kappa - \left[(\varepsilon - \tilde{\varepsilon})/8\pi\right]E^2 - \left(4\pi/\tilde{\varepsilon}\right)\sigma_0/\tilde{\varepsilon} \qquad (2)$$

where γ is the surface tension, κ is twice the mean curvature of the interface, $\varepsilon/(4\pi)$ is the permittivity constant in the jet, $\tilde{\varepsilon}/(4\pi)$ is the permittivity constant in the air and σ is the surface free charge.

Following the previous investigation Hohman et al.(2001a), we consider a cylindrical fluid jet moving axially. The fluid of air is considered as the external fluid, and the internal fluid

of jet is assumed to be Newtonian and incompressible. We use the governing equations (1) in the cylindrical coordinate system with origin at the center of nozzle exit section, where the jet flow is emitted with axial z-axis along the axis of the jet. We consider the axisymmetric form of the dependent variables in the sense that the azimuthal velocity is zero and there are no variations of the dependent variables with respect to the azimuthal variable. Following approximations carried out in Hohman et al.(2001a) for a long and slender jet in the axial direction, we consider length scale in the axial direction to be large in comparison to that in the radial direction and use a perturbation expansion in the small jet' aspect ratio. We expand the dependent variables in a Taylor series in the radial variable r. Then such expansions are used in the full axisymmetric system and keep only the leading terms. These lead to relatively simple equations for the dependent variables as functions of t and z only. Following the method of approach in Hohman et al.(2001a) , we employ (1d) and Coulomb's integral equation to arrive at an equation for the electric field, which is essentially as the one derived by Hohman et al.(2001a) and will not be repeated here.

We non dimensionalize the resulting equations using r_0 (radius of the cross sectional area of the nozzle exit at z=0), $E_0 = \sqrt{\frac{\gamma}{(\varepsilon - \tilde{\varepsilon})r_0}}$, $t_0 = \sqrt{\frac{\rho r_0}{\gamma}}$, $\frac{r_0}{t_0}$ and $\sqrt{\frac{\gamma\tilde{\varepsilon}}{r_0}}$ as scales for length, electric field, time, velocity and surface charge, respectively. The resulting non-dimensional equations are then

$$\frac{\partial}{\partial t}\left(h^2\right) + \frac{\partial}{\partial z}\left(h^2 v\right) = 0 \tag{3a}$$

$$\frac{\partial}{\partial t}\left(h\sigma\right) + \frac{\partial}{\partial z}\left(hv\varsigma\right) + \frac{1}{2}\frac{\partial}{\partial z}\left(h^2 EK\right) = 0 \tag{3b}$$

$$\frac{\partial v}{\partial t}+v\frac{\partial v}{\partial z}=-\frac{\partial}{\partial z}\left[\frac{h}{\sqrt{1+\left(\frac{\partial h}{\partial z}\right)^2}}-\frac{\frac{\partial^2 h}{\partial z^2}}{\sqrt[3]{1+\left(\frac{\partial h}{\partial z}\right)^2}}-\frac{E^2}{8\pi}-4\pi\sigma^2\right]$$

$$+\frac{2E\sigma}{h\sqrt{\beta}}+\frac{3\nu^*}{h^2}\frac{\partial}{\partial z}\left(h^2\frac{\partial v}{\partial z}\right) \qquad (3c)$$

$$E_b(z)=E-\ln(\chi)\left[\frac{\beta}{2}\frac{\partial^2}{\partial z^2}\left(h^2E\right)-4\pi\sqrt{\beta}\frac{\partial}{\partial z}\left(h\sigma\right)\right] \qquad (3d)$$

where v is the axial velocity, h(z, t) is the radius of the jet' cross-section at the axial location z, σ(z, t) is the surface charge, E(z, t) is the electric field, the conductivity K is assumed to be a function of z in the form $K=K_0\tilde{K}(z)$, where K_0 is a constant dimensional conductivity and $\tilde{K}(z)$ is a non-dimensional variable function. Also, non-dimensional conductivity is given by $K^*=K_0\sqrt{\frac{\rho r_0^3}{\gamma\beta\tilde{\varepsilon}^2}}$ and $\beta=\frac{\varepsilon}{\tilde{\varepsilon}}-1$. Also $\nu^*=\sqrt{\frac{\nu_0^2\rho r_0}{\gamma}}$ is the non-dimensional viscosity parameter, $E_b(z)$ is an applied electric field and $\frac{1}{\chi}$ is the local aspect ratio, which is assumed to be small.

1.3 Perturbation Analysis

Next, we determine the electrostatic equilibrium solution, which is referred to here as the basic state solution, to the equations (3a-3d). The basic state solutions for the dependent variables, which are designated with a subscript '*b*', are given below

$$h_b = 1, \quad v_b = v_0, \quad \sigma_b = \sigma_0, \quad E_b = \Omega_0 (1\text{-}\delta z), \qquad \text{(4a-d)}$$

where both v_0, σ_0 and Ω_0 are constant quantities, and $\delta = 8\sigma_0\pi/(\Omega\sqrt{\beta})$ is assumed to be a small parameter ($\delta << 1$), under which the basic state solutions given by (4a-d) were found to satisfy the modeling equations , Riahi(2009). Here σ_0 is referred to as the background free charge density. We consider each dependent variable as sum of its basic state solution plus a small perturbation, which is assumed to be oscillatory in time and in axial variable. Thus, we write

$$(h, v, \sigma, E) = (h_b, v_b, \sigma_b, E_b) + (h_1, v_1, \sigma_1, E_1) \qquad \text{(5a)}$$

where the perturbation quantities, designated by the subscript '1', are given by

$$(h_1, v_1, \sigma_1, E_1) = (\tilde{h}, \tilde{v}, \tilde{\sigma}, \tilde{E}) e^{\omega t + ikz} \qquad \text{(5b)}$$

Here $(\tilde{h}, \tilde{v}, \tilde{\sigma}, \tilde{E})$ are constants which are assumed to be small, i is the imaginary unit, ω is the complex growth rate, and k is the axial wave number. Using (4)-(5) in (3), we linearize with respect to the amplitude of perturbation, consider a series expansion in powers of δ for all the dependent variable and only retain the lowest leading order terms, and then divide each equation by the exponential function $\exp[\omega t + ikz]$. We then obtain 4 linear algebraic equations for the unknown constants $(\tilde{h}, \tilde{v}, \tilde{\sigma}, \tilde{E})$. To obtain non-trivial (non-zero) values of these constants, the 4x4 determinant of the coefficients of these unknowns must be zero, which yields the following dispersion relation.

1.4 Dispersion Relation

$$\omega^3 + T_1\omega^2 + T_2\omega + T_3 = 0 \tag{6}$$

where

$$T_1 = 3k\left(\nu^* k + i\nu_b\right) + \frac{4\pi K^*\Lambda}{\delta\sqrt{\beta}} \tag{7}$$

$$T_2 = k^2\left[\frac{k^2-1}{2} + \frac{12\pi\nu^* K^*\Lambda}{\delta\sqrt{\beta}} + 4\pi\sigma_b^2\left(\frac{4\Gamma}{\delta} - 1\right) + \frac{E_b^2\Lambda}{4\pi\delta}\right.$$

$$\left. + i\nu_b\left(3i\nu_b + 6k\nu^* + \frac{8\pi K^*\Lambda}{k\delta\sqrt{\beta}}\right)\right] \tag{8}$$

$$T_3 = \frac{4\pi k^2 K^*\Lambda}{\delta\sqrt{\beta}}\left[\frac{k^2-1}{2} + \frac{E_b^2\delta}{4\pi\Lambda} + 4\pi\sigma_b^2 + \frac{2i\sigma_b E_b}{k\sqrt{\beta}}\left(\frac{1}{\Gamma} - 2\right)\right]$$

$$+ ik^3\nu_b\left[\frac{k^2-1}{2} + \frac{E_b^2\Lambda}{4\pi\delta} + 4\pi\sigma_b^2\left(\frac{4\Gamma}{\delta} - 1\right) + \frac{12\pi\nu^* K^*\Lambda}{\delta\sqrt{\beta}}\right]$$

$$- k^2\nu_b^2\left[3\nu^* k^2 + \frac{4\pi K^*\Lambda}{\delta\sqrt{\beta}} + ik\nu_b\right] \tag{9}$$

with $\chi = \dfrac{1}{0.89k}$, $\Gamma = \ln(\chi)$, $\Lambda = \beta k^2\Gamma$, $\delta = \Lambda + 2$.

1.5 Results and Discussion

The dispersion relation (6) which presents the temporal behavior of the system is investigated for several parameters. For all our computational purpose, we use $\beta = 77$

Our aim here is to present the positive real part and the imaginary part of the solution ω of the equation (6), which is called, respectively, the growth rate and the frequency of the unstable mode, and these contributes to our understanding of the temporal instability. From our computational results (see APPENDIX A), it is observed that the positive real part of ω is independent of the basic state velocity v_b, only the imaginary part depends on v_b. All the parameters we choose yielded negative imaginary part for nonzero basic state velocity.

Figure 2 through 4 present results for constant applied field and for various values of E_b. Here we consider four values 0.0, 0.97, 1.93 and 2.9. Results in figure 2 are for infinite conductivity case, i.e., $K^* = \infty.$ other parameters chosen as $v_b = 1,\ \nu^* = 0, \sigma_b = 0.$

As can be seen from the figure 2, the instability is reduced with increasing the magnitude of the applied field. The results indicate presence of the electrically analog of the so-called Rayleigh mode of instability Drazin (1981). The results presented in the figure 2 are also in qualitative agreement with those reported in Hohman et al. (2001a) for a perfect conducting fluid case and zero basic state velocity.

Results for zero conductivity, i.e., $(K^* = 0)$, and $K^* = 19.3$ cases are presented in figure 3 and figure 4 respectively keeping other parameters same as in the figure 2.
As in the case of perfect conducting fluid, the results for the perfect dielectric fluid cases shown in the figure 3 indicate that the flow instability is reduced with increasing the magnitude of the applied field, which is again a property of the Rayleigh type mode of jet instability. The results presented in the figure 4 for a finite conducting case are qualitatively similar to those presented in the figures 2-3 and indicate those results for Rayleigh type mode of instability.

Figure 5 presents some results for the constant applied field and compares the positive real solutions for three different conductivity cases, namely, zero, infinite and finite (19.3) for $E_b = 2.9, \nu^* = 0, \sigma_b = 0$ and $v_b = 1$. It is noticed that the results are closed to each other for $K^* = 19.3,$ and $K^* = \infty.$ it is seen from the figure 5 the stability effect due to conductivity of the fluid.

The effect of ν^* is shown in figure 6 for zero and finite conductivities. Other parameters used are $E_b = 2.9,\ \sigma_b = 0$ and $v_b = 1$. Again the case of constant applied field is considered here. It can be seen from the results presented in the figure 6 that both viscosity and conductivity reduce the instability of the unstable mode.

The effect of surface charge is presented next. Figure 7 displays the effect of σ_b for zero conductivity with $E_b = 2.9,\ \nu^* = 0$ and $v_b = 1$. It is seen from the results shown in the figure 7 that surface charge density enhances the instability of the unstable mode for the axial wave number not too close to zero; while the opposite is true if the wave number is sufficiently small.

Figure 8 presents results for variable applied field, finite and nonzero viscosity and conductivity and for different values of the strength of the applied field. It can be seen from the results shown in the figure 8 that the instability mode favors intermediate values of the axial wave number (not too close to zero or one values).

It is observed from numerical investigations that there are two modes of instability for small values of *k*. The primary mode dominates the secondary mode. The secondary mode exists only for small values of *k*. The secondary mode also independent of basic state velocity, i.e., real part of ω does not depend on the basic state velocity which is the case for primary mode also. The secondary modes are presented in figure 9 with $K^* = 19.3, \nu^* = 0, \sigma_b = 0.1, \ \ v_b = 1$ for various E_b.

A comparison of these two modes are shown in figure 10 for $K^* = 19.3, \nu^* = 0, \sigma_b = 0.1,$ $v_b = 1$ and $E_b = 2.9$. For very small values of *k*, the secondary mode exists whereas for larger *k*, this mode does not exist. For larger values of *k*, only one mode (namely, primary mode) exists. Figure 11 through figure 13 presents the imaginary part of the frequency of the unstable mode versus the axial wave number for zero conductivity and finite conductivity. Other parameters varied are viscosity and basic state velocity. It can be seen from the figure 11 that the period of the unstable mode is smaller for larger value of the basic state velocity and decreases with increasing the axial wave number of the unstable mode. Also, rate of increase of the frequency of the unstable mode with respect to the axial wave number increases with the basic state velocity. It can be seen from the figure 12 that the imaginary part of ω of the unstable mode for finite conductivity and zero viscosity case has sudden change in magnitude when k is close to 0.68.

Figure 13 presents the results for imaginary part of ω with $K^* = 19.3, \nu^* = 0.333, \sigma_b = 0.1,$ and $E_b = 2.9$ for various basic state velocities. These is no unstable mode for *k* approximately bigger than 0.5.

1.6 Temporal Instability Figures

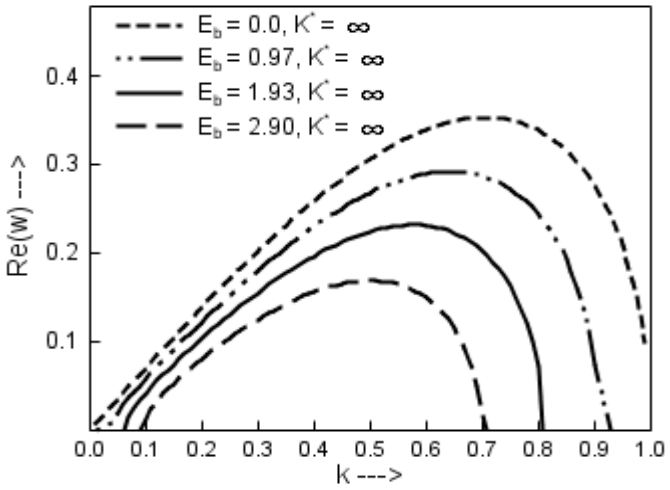

Figure 2. Positive real part of ω as a function *k* with $K^* = \infty, \nu^* = 0, \sigma_b = \sigma_0 = 0$ And $\nu_b = \nu_0 = 1$ for various $E_b (= \Omega_0)$.

Figure 3. Positive real part of ω as a function *k* with $K^* = 0, \nu^* = 0, \sigma_b = 0$ And $\nu_b = 1$ for various E_b.

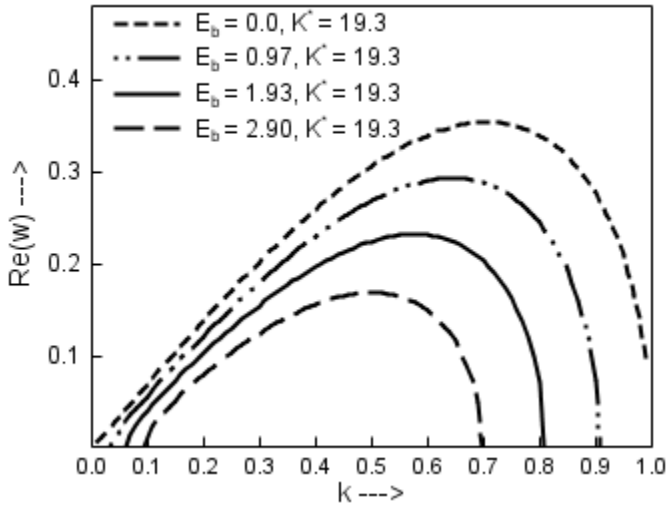

Figure 4. Positive real part of ω as a function *k* with $K^* = 19.3, \nu^* = 0, \sigma_b = 0$ And $\nu_b = 1$ for various E_b.

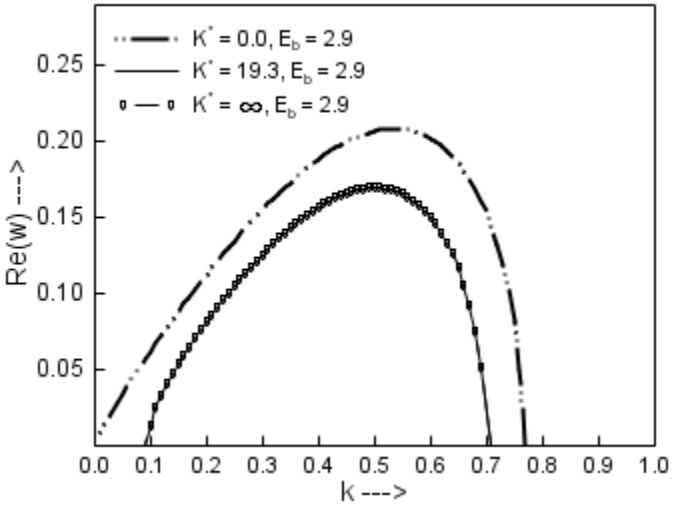

Figure 5. Positive real part of ω as a function *k* with $E_b = 2.9, \nu^* = 0, \sigma_b = 0$ And $\nu_b = 1$ for various K^*.

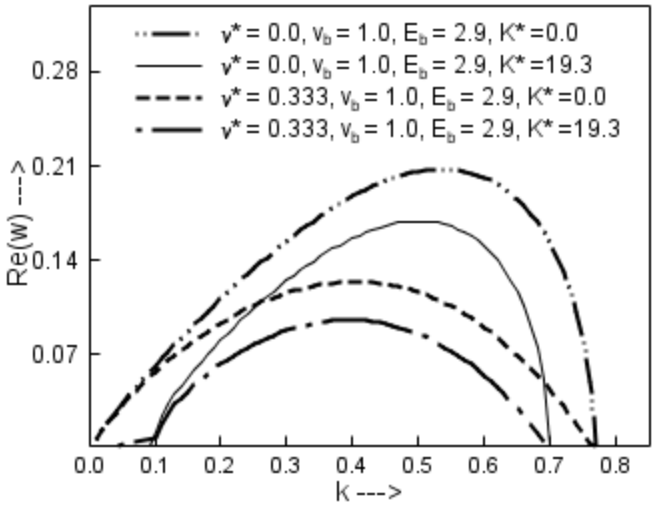

Figure 6. Positive real solutions of ω as a function *k* with $\sigma_b = 0$ And $v_b = 1$ for various ν^* *and* K^*.

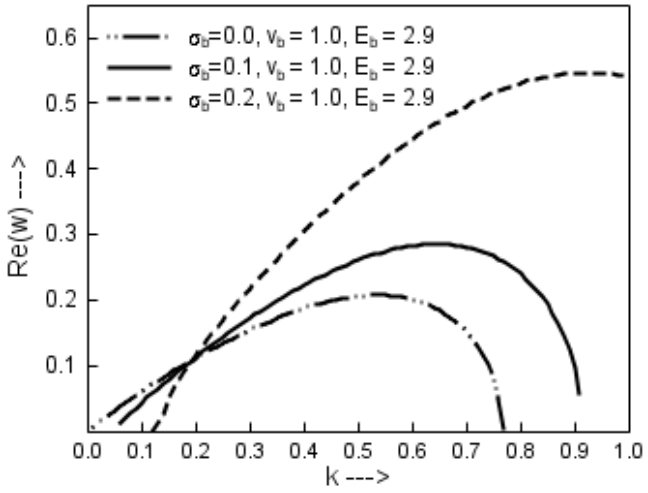

Figure 7. Positive real solutions of ω as a function *k* with $K^* = 0, \nu^* = 0, E_b = 2.9$ And $v_b = 1$ for various σ_b.

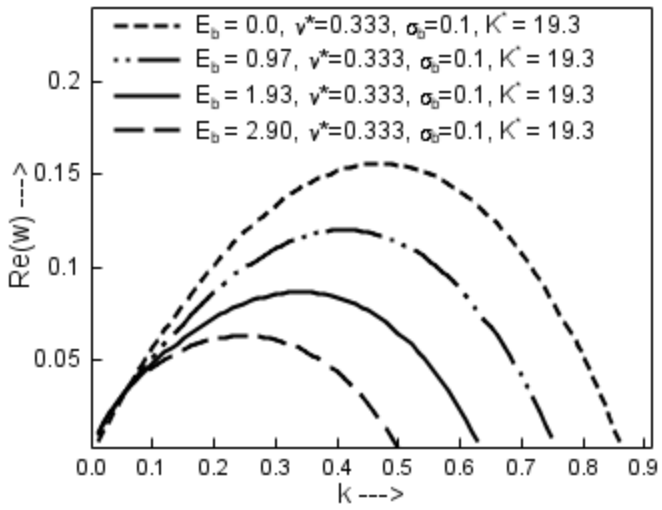

Figure 8. Positive real solutions of ω as a function *k* with $K^* = 19.3, \nu^* = 0.333, \sigma_b = 0.1$ And $\nu_b = 1$ for various E_b.

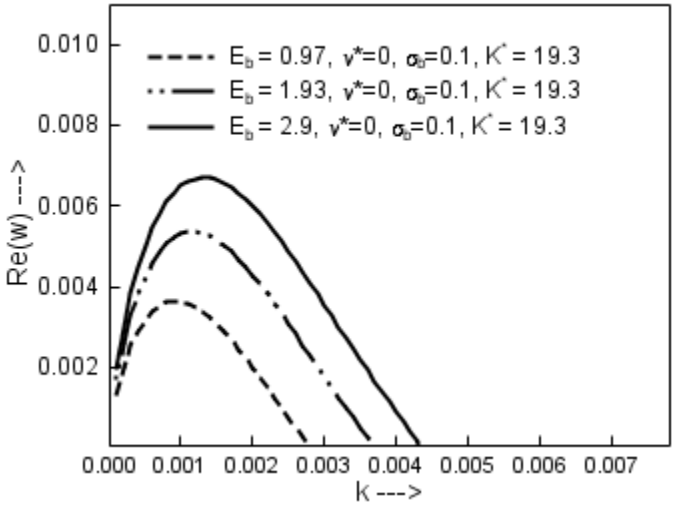

Figure 9. Secondary mode: positive real solutions of ω as a function *k* with $K^* = 19.3, \nu^* = 0, \sigma_b = 0.1,$ And $\nu_b = 1$ for various E_b.

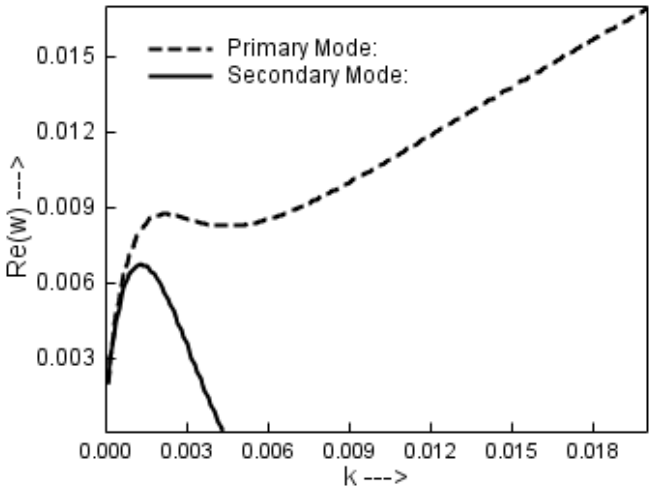

Figure 10. Primary and Second modes with
$K^* = 19.3, \nu^* = 0, \sigma_b = 0.1,\ v_b = 1$ And $E_b = 2.9$

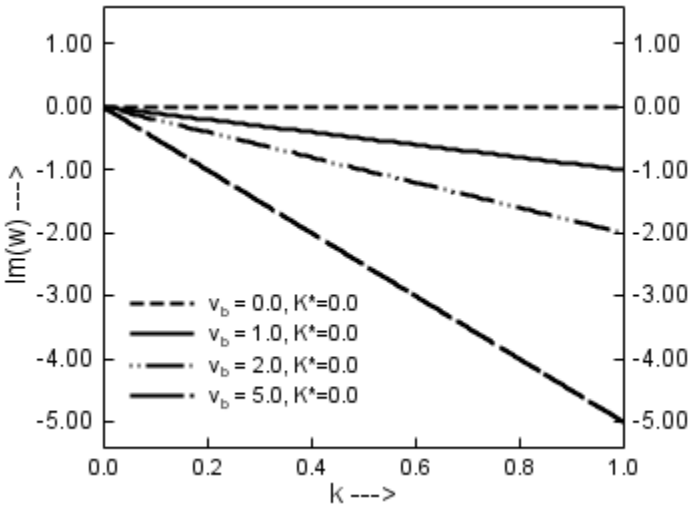

Figure 11. Imaginary part of ω whose real part is positive
with $K^* = 0, \nu^* = 0, \sigma_b = 0.1, E_b = 2.9$.

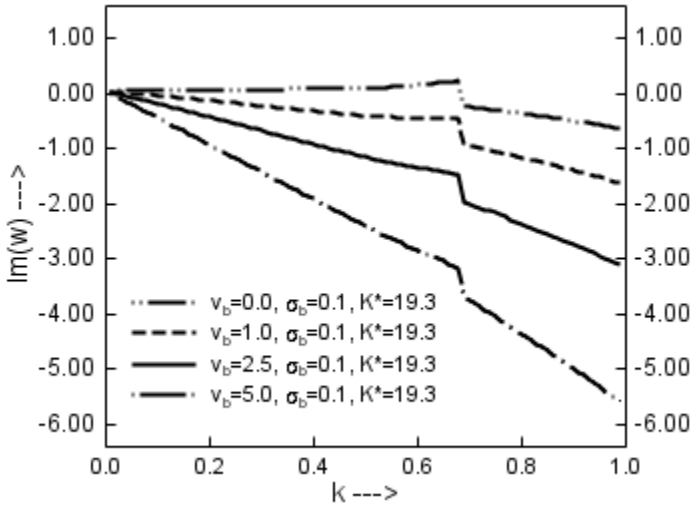

Figure 12. Imaginary part of ω whose real part is positive with $K^* = 19.3, \nu^* = 0.0, \sigma_b = 0.1, E_b = 2.9$

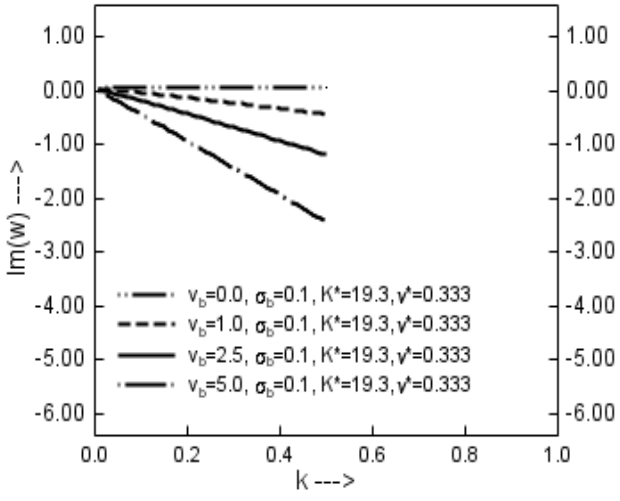

Figure 13. Imaginary part of ω whose real part is positive with $K^* = 19.3, \nu^* = 0.333, \sigma_b = 0.1, E_b = 2.9$.

1.7 Concluding Remarks

We conclude that in the realistic cases of the non-zero basic state velocity, the growth rate of the unstable mode is unaffected by the value of the basic state velocity. However, the non-zero value of the basic state velocity affects significantly the period of the unstable mode in the sense that it decreases the period, and the rate of increase of the frequency with respect to the axial wave number increases with the basic state velocity. In all the cases that we investigated we found that the presence of the variable applied field is destabilizing, while the finite values of either viscosity or conductivity are stabilizing. It is also noticed for the zero conductivity case that the imaginary part of ω is zero if basic state velocity is zero and the imaginary part of ω is nonzero if basic state velocity is nonzero. It is also observed from numerical investigations that there are two modes of instability for small values of the wavenumber. The primary mode dominates the secondary mode. The secondary mode exists only for small values of *k*. The secondary mode also independent of basic state velocity, i.e., real part of ω does not depend on the basic state velocity which is the case for primary mode also.

CHAPTER II

SPATIAL INSTABILITY

This chapter considers the problem of spatial instability of a cylindrical viscous jet of fluid with zero and infinite electrical conductivity, a static charge density and in the presence of an external variable electric field. The investigations of electrically forced jets are important particularly in applications such as those to electro spraying, Baily (1981), and electro spinning, Hohman et al (2001a-b). Electro spinning is a technology that uses electric fields to produce and control small fibers. The aim is at producing non-woven materials that are unparalleled in their porosity, high surface area, and the fineness and uniformity of their fibers. Electro spraying is a technology that uses electric field to produce and control sprays of very small drops. The aim is at producing very small drops that are uniform in size and are of charged macromolecules in the gas phase. Without presence of electrical field effects, it is known for several decades that spatially growing disturbances are, in general, more appropriate and realized than the temporally growing counterparts for the jet flows and other types of free shear flows Drazin (1981). For example, Michalke (1965), studied instability of the free shear layers and found that theoretical results based on the spatial instability have better agreement with the corresponding experimental results. Later, additional investigations of spatial instability of free shear flows and jets were reported by a number of authors including those by Monkewitz (1982), Lie (1988), Tam (1993),

Soderberg (2003) and Healey (2008). Soderberg (2003) showed, in particular, agreement between the linear spatial instability results and the corresponding experimental results.

For the jet flows driven by the electric forces, temporal instability of such flows has been studied theoretically by several authors including Hohman et al.(2001a) , Reneker et al.(2000) , Shkadov (2001), Fridrikh et al.(2003) , Bhatta et al.(2010), Hohman et al.(2001a) studied the linear temporal instability of an electrically forced jet with uniform applied field. The simplified equations for the dependent variables of the disturbances that they analyzed were based on the long wavelength and asymptotic approximations of the original electro-hydrodynamic equations. For the axisymmetric jets, the authors detected, in particular, two temporal instability modes, independence of temporal instability on the basic state velocity, and also they discussed the properties of such instability modes in the various possible limits. Other investigations of the problems dealing with the electrically forced jets with applications in electro spinning of nano fiber are reported in several papers including Sun et al.(2003) , Li (2004) , Yu et al.(2004).

Recently, Riahi (2009) considered electrically forced jets with variable applied field. He followed a modeling approach analog to that due to, Hohman et al. (2001a) and investigated analytically spatial instability of axisymmetric jets under idealistic conditions of either jet of zero electrical conductivity or jet of infinite electrical conductivity and subjected to certain restrictions on the frequency of the disturbances. He detected two spatial modes of instability each of which was enhanced with increasing the strength of the externally imposed applied electric field. These modes existed under certain restricted ranges of the axial wave number of disturbances, but, in particular, one of the modes did not exist if the axial wave number was sufficiently large.

2.1 Spatial Instability Case

In the present study we first use a method of approach similar to that employed by Riahi (2009) to arrive at a mathematical model for the non-idealistic (realistic) electrically driven viscous jets with zero and infinite conductivity. Next, we consider spatial instability of the jets for externally imposed variable applied field and non-zero basic state velocity. We then determine a rather lengthy dispersion relation, which relates the growth rate of the spatially growing disturbances to the wave number in the axial direction, the frequency and the non-dimensional parameters of the model. We solve numerically the dispersion relation for the growth rate and frequency of the disturbances.

2.2 Mathematical Formulation

We use the original governing electro-hydrodynamic equations, Melcher J. R., and Taylor G. I. (1969) for the mathematical modeling of the electrically driven jets. The system is governed by,

$$\frac{D\rho}{Dt} + \rho\nabla.\vec{u} = 0 \tag{1a}$$

$$\rho\frac{D\vec{u}}{Dt} = -\nabla P + \nabla.\nabla\left(\mu\vec{u}\right) + q\vec{E} \tag{1b}$$

$$\frac{Dq}{Dt} + \nabla.\left(K\vec{E}\right) = 0 \tag{1c}$$

$$\vec{E} = -\nabla\Phi \tag{1d}$$

where $\frac{D}{Dt} = \frac{\partial}{\partial t} + \vec{u}.\nabla$ is the total derivative. Here $\vec{u}$ is the velocity vector, P is the pressure, $\vec{E}$ is the electric field vector, Φ is the electric potential, q is the free charge density, ρ is the fluid density, μ is the dynamic viscosity, K is electric conductivity and t is the time variable. The geometry we use is shown in figure 1.

The internal pressure in the jet can be found by taking into consideration the balances across the free boundary of the jet between the pressure, viscous forces, capillary forces and the electric energy density plus the radial self-repulsion of the free charges on the free boundary G.I Taylor (1969). Assuming the ambient air to be motionless and passive, this yield the following expression for the pressure P in the jet

$$P = \gamma\kappa - \left[(\varepsilon - \tilde{\varepsilon})/8\pi\right]E^2 - \left(4\pi/\tilde{\varepsilon}\right)\sigma_0/\tilde{\varepsilon} \qquad (2)$$

where γ is the surface tension, κ is twice the mean curvature of the interface, $\varepsilon/(4\pi)$ is the permittivity constant in the jet, $\tilde{\varepsilon}/(4\pi)$ is the permittivity constant in the air and σ is the surface free charge.

Following the previous investigation Hohman et al. (2001a), we consider a cylindrical fluid jet moving axially. The fluid of air is considered as the external fluid, and the internal fluid of jet is assumed to be Newtonian and incompressible. We use the governing equations (1) in the cylindrical coordinate system with origin at the center of nozzle exit section, where the jet flow is emitted with axial z-axis along the axis of the jet. We consider the axisymmetric form of the dependent variables in the sense that the azimuthal velocity is zero and there are no variations of the dependent variables with respect to the azimuthal variable. Following approximations carried out in Hohman et al.(2001a) for a long and slender jet in the axial direction, we consider length scale in the axial direction to be large in comparison to that in the radial direction and use a

perturbation expansion in the small jet' aspect ratio. We expand the dependent variables in a Taylor series in the radial variable r. Then such expansions are used in the full axisymmetric system and keep only the leading terms. These lead to relatively simple equations for the dependent variables as functions of t and z only. Following the method of approach in Hohman et al.(2001a), we employ (1d) and Coulomb's integral equation to arrive at an equation for the electric field, which is essentially as the one derived by Hohman et al.(2001a) and will not be repeated here.

We non dimensionalize the resulting equations using r_0 (radius of the cross sectional area of the nozzle exit at z=0), $E_0 = \sqrt{\frac{\gamma}{(\varepsilon - \tilde{\varepsilon})r_0}}$, $t_0 = \sqrt{\frac{\rho r_0}{\gamma}}$, $\frac{r_0}{t_0}$ and $\sqrt{\frac{\gamma\tilde{\varepsilon}}{r_0}}$ as scales for length, electric field, time, velocity and surface charge, respectively. The resulting non-dimensional equations are then

$$\frac{\partial}{\partial t}\left(h^2\right)+\frac{\partial}{\partial z}\left(h^2 v\right)=0 \tag{3a}$$

$$\frac{\partial}{\partial t}\left(h\sigma\right)+\frac{\partial}{\partial z}\left(hv\varsigma\right)+\frac{1}{2}\frac{\partial}{\partial z}\left(h^2 EK\right)=0 \tag{3b}$$

$$\frac{\partial v}{\partial t}+v\frac{\partial v}{\partial z}=-\frac{\partial}{\partial z}\left[\frac{h}{\sqrt{1+\left(\frac{\partial h}{\partial z}\right)^2}}-\frac{\frac{\partial^2 h}{\partial z^2}}{\sqrt[3]{1+\left(\frac{\partial h}{\partial z}\right)^2}}-\frac{E^2}{8\pi}-4\pi\sigma^2\right]$$

$$+\frac{2E\sigma}{h\sqrt{\beta}}+\frac{3\nu^*}{h^2}\frac{\partial}{\partial z}\left(h^2\frac{\partial v}{\partial z}\right) \tag{3c}$$

$$E_b(z)=E-\ln(\chi)\left[\frac{\beta}{2}\frac{\partial^2}{\partial z^2}\left(h^2 E\right)-4\pi\sqrt{\beta}\frac{\partial}{\partial z}\left(h\sigma\right)\right] \tag{3d}$$

where v is the axial velocity, h (z, t) is the radius of the jet' cross-section at the axial location z, σ(z, t) is the surface charge, E (z, t) is the electric field, the conductivity K is assumed to be a function of z in the form $K=K_0\tilde{K}(z)$, where K_0 is a constant dimensional conductivity and $\tilde{K}(z)$ is a non-dimensional variable function. Also, non-dimensional conductivity is given by $K^* = K_0\sqrt{\frac{\rho r_0^{\,3}}{\gamma\beta\tilde{\varepsilon}^2}}$ and $\beta = \frac{\varepsilon}{\tilde{\varepsilon}} - 1$. Also $\nu^* = \sqrt{\frac{\nu_0^{\,2}\rho r_0}{\gamma}}$ is the non-dimensional viscosity parameter, $E_b(z)$ is an applied electric field and $\frac{1}{\chi}$ is the local aspect ratio, which is assumed to be small.

2.3 Perturbation Analysis

Next, we determine the electrostatic equilibrium solution, which is referred to here as the basic state solution, to the equations (3a-3d). The basic state solutions for the dependent variables, which are designated with a subscript '*b*', are given below

$$h_b = 1, \quad v_b, \quad \sigma_b, \quad E_b = \Omega_0(1-\delta z), \qquad \text{(4a-4d)}$$

Where v_b, σ_b and Ω_0 are constant quantities, and $\delta=8\sigma_b\pi/(\Omega\sqrt{\beta})$ is assumed to be a small parameter ($\delta<<1$), under which the basic state solutions given by (4a-4d) were found to satisfy the modeling equations, Riahi(2009) . Here σ_b is referred to as the background free charge density. We consider each dependent variable as sum of its basic state solution plus a small perturbation, which is assumed to be oscillatory in time and in axial variable.

Thus, we write

$$(h, v, \sigma, E) = (h_b, v_b, \sigma_b, E_b) + (h_1, v_1, \sigma_1, E_1) \tag{5a}$$

where , perturbation quantities are designated by the subscript '1', are given by

$$(h_1, v_1, \sigma_1, E_1) = (\tilde{h}, \tilde{v}, \tilde{\sigma}, \tilde{E}) e^{i\omega t + (s+ik)z} \tag{5b}$$

Here $(\tilde{h}, \tilde{v}, \tilde{\sigma}, \tilde{E})$ are constants which are assumed to be small, *i* the imaginary unit, ω is the frequency and s is the real growth rate of the spatially growing disturbances, and *k* is the axial wave number.

2.4 Dispersion Relation

Using equations (4)-(5) in (3), we linearize with respect to the amplitude of perturbation, consider a series expansion in powers of δ for all the dependent variable and only retain the lowest leading order terms, and then divide each equation by the exponential function exp [$i\omega t+(s+ik)\ z$]. We then obtain four linear algebraic equations for the unknown constants $(\tilde{h}, \tilde{v}, \tilde{\sigma}, \tilde{E})$. To obtain non-trivial (non-zero) values of these constants, the 4x4 determinant of the coefficients of these unknowns must be zero, which yields the following dispersion relation:

$$T_1\omega^3 - iT_2\omega^2 - T_3\omega + iT_4 = 0 \tag{6}$$

where,

$$T_1 = 2 - \beta(s+ik)^2\Gamma$$

(6a)

$$T_2 = [2(s+ik)\nu_b - T_{32}]T_1 - 4\pi\sqrt{\beta}K^*(s+ik)^2\Gamma \tag{6b}$$

$$\begin{aligned} T_3 &= (s+ik)[(s+ik){\nu_b}^2 + \frac{T_{31}}{2} + \frac{\sigma_b T_{33}}{2} - 2\nu_b T_{32}]T_1 \\ &\quad - 4\pi\sqrt{\beta}K^*(s+ik)\Gamma[\sigma_b T_{34} - K^* T_{32} + \nu_b(s+ik)K^*] - T_{34}T_{41}\Gamma \end{aligned} \tag{6c}$$

$$\begin{aligned} T_4 &= (s+ik)[(s+ik)\nu_b\{\sigma_b T_{33} - \nu_b T_{32} + \frac{T_{31}}{2}\}] - \frac{T_{21}T_{33}T_1}{2} \\ &\quad + 2(s+ik)^2 K^*\Gamma[\frac{T_{33}T_{41}}{4} + (s+ik)\pi\sqrt{\beta}](2\nu_b T_{32} - T_{31}) \\ &\quad + 2(s+ik)^2\Gamma T_{34} 2\pi\sqrt{\beta}[T_{21} - 2(s+ik)\nu_b\sigma_b] - \frac{\nu_b T_{41}}{2} \end{aligned} \tag{6d}$$

with

$$T_{34} = \frac{2\sigma_b}{\sqrt{\beta}} + \frac{E_b(s+ik)}{4\pi}$$

$$T_{41} = (s+ik)(4\pi\sigma_b\sqrt{\beta}) - \beta(s+ik)E_b$$

$$T_{31} = (s+ik)[1+(s+ik)^2] - \frac{2\sigma_b E_b}{\sqrt{\beta}}$$

$$T_{21} = (s+ik)(\sigma_b E_b + K^* E_b)$$

$$T_{33} = 8\pi\sigma_b(s+ik) + \frac{2E_b}{\sqrt{\beta}}$$

$$T_{32} = (s+ik)[3\nu^*(s+ik) - \nu_b]$$

$$T_{44} = \frac{1}{\Gamma} - \frac{\beta(s+ik)^2}{2}$$

and ,

$$\chi = \frac{1}{0.89k}, \quad \Gamma = \ln(\chi), \quad \Lambda = \beta k^2\Gamma, \quad \delta = \Lambda + 2 \tag{6e}$$

2.5 Results and Discussion

The dispersion relation (6) which presents the spatial behavior of the system is investigated as function of several parameters. For all our computational (see Appendix B) purpose, we use various parameters from (6e) used by Hohman et al. (2001a) Our aim here is to present the positive real part of s and the real part of the solution ω of the equation (6), which is respectively called as the spatial growth rate and the frequency of the unstable mode and these contributes to the spatial instability. We solve the dispersion relation numerically.

Figures 14 through 16 present results for constant applied field and for various values of E_b. Here we consider four values 0.0, 1.0, 1.5 and 2.0. Results in figure 2 are for zero conductivity case, i.e. K*=0, other parameters chosen as $v_b = 3,\ \nu^* = 0, \sigma_b = 0.$

As can be seen from the figure 14, the instability is reduced with increasing the magnitude of the applied field. The results indicate presence of the electrically analog of the so-called Rayleigh mode of instability, Drazin (1981). The results presented in the figure 14 are also in qualitative agreement with those reported in, Hohman et al. (2001a) for a perfect conducting fluid case and zero basic state velocity. Results for zero conductivity, i.e., $(K^* = 0)$, and different v_b cases are presented in figure 15 keeping other parameters same as in the figure 14.

As in the case of perfect conducting fluid, the results for the perfect dielectric fluid cases shown in the figure 15 indicate that the flow instability is reduced with increasing the magnitude of the basic state velocity, which appears to be due to the effect of non-zero basic state velocity of the jet with zero conductivity. In this case, higher value of the basic state velocity makes the jet more stable versus the spatially growing perturbation.

The results presented in the figure 16 for a zero conducting case are in agreement with those in the figure 15 for the stabilizing effect of the basic state velocity in the sense that the period of the unstable mode increases with basic state velocity. In addition, as can be seen in this figure and all the rest of our generated data for the frequency of the unstable mode, the frequency is negative which indicates that the spatially growing perturbation moves axially in the positive direction with increasing value of the axial variable.

Figure 17 presents some results for the variable applied field and compares the positive real growth rates for infinite conductivity case with $E_b = 1.0, \nu^* = 0.3333, \sigma_b = 0.01$ and various v_b . It is seen from the figure 17 the instability increases due to increase in basic state velocity, and it is also seen that basic state velocity dominates the effect of other parameters. Thus, basic state velocity can enhance perturbation growth when the jet's conductivity is sufficiently high.

The effect of ν^* is shown in figure 6 for jets with infinite conductivities and variable applied field. Other parameters used are $E_b = 1.0,\ \sigma_b = 0.01$ and $v_b = 1$. It can be seen from the results presented in the figure 18 that viscosity reduces the stability of the unstable mode. This is a consequence of spatially growing jets with non-zero basic state velocity in agreement with the non-electric free shear layer , Drazin (1981), where viscous instability modes were found to be more unstable than the corresponding in viscid modes Lie (1988).

The effect of dominance of basic state velocity is presented next. Figure 7 displays the effect of ν^* for infinite conductivity with $E_b = 1.0$ and $v_b = 0$. Comparing the results shown in the figure 19& Figure 18 it is clear that viscosity is stabilizing when v_b is absent but when v_b is present, it clearly dominates over the viscosity effect and enhances the instability of the unstable mode.

Figure 8 presents results for variable applied field, finite and nonzero viscosity and background free charge density and for different values of the strength of the applied field. It can be seen from the results shown in the figure 20 that the instability mode decreases with increase in applied field, the basic state velocity being small in magnitude. We refer to the mode of instability here as the secondary one since the value of the corresponding growth rates are small as compared to those for primary mode presented in the next figure.

Now, we will see the presence of new type of mode, refers to here as the primary one, which is more significant than the secondary one since it exhibits relatively larger growth rates and in the presence of non-zero basic state velocity. Figure 21 presents the contrasting results for variable applied field, finite and nonzero viscosity and background free charge density and for different values of the strength of the applied field with non-zero value of the basic state velocity. It can be compared from the results shown in the figures 20 and 21 that clearly the primary instability mode is weaker than the corresponding secondary one.

Thus, as is observed from the numerical investigations described above, there can be two modes of instability. The primary mode dominates over the secondary mode. The two modes are presented in figure 22 with $K^* = \infty, \nu^* = 0.333, \sigma_b = 0.01, \ v_b = 1$ for $E_b = 0$.

For very small values of *k*, only the primary mode exists whereas for larger *k*, both modes of instability can operate, even though the primary mode is the most dangerous one. Figure 23 presents the magnitude of the frequency of the unstable mode versus the axial wave number for infinite conductivity. Other parameter varied is the basic state velocity. It can be seen from the figure 23 that the period of the unstable mode is smaller for larger value of the basic state velocity and decreases with increasing the axial wave number of the unstable mode. Also, rate of

increase of the frequency of the unstable mode with respect to the axial wave number increases with the basic state velocity.

From the figure 24 it is observed that the maximum growth rate corresponds to value of the perturbation's period which is relatively not too large and not too small.

2.6 Spatial Instability Figures

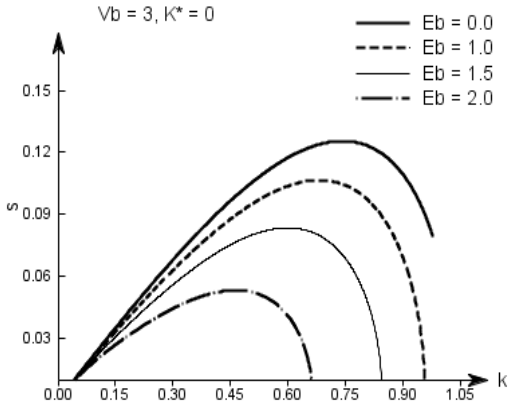

Figure 14. Positive real part of s as a function k with $K^* = 0, \nu^* = 0, \sigma_b = 0$ and $v_b = 3$ for various E_b.

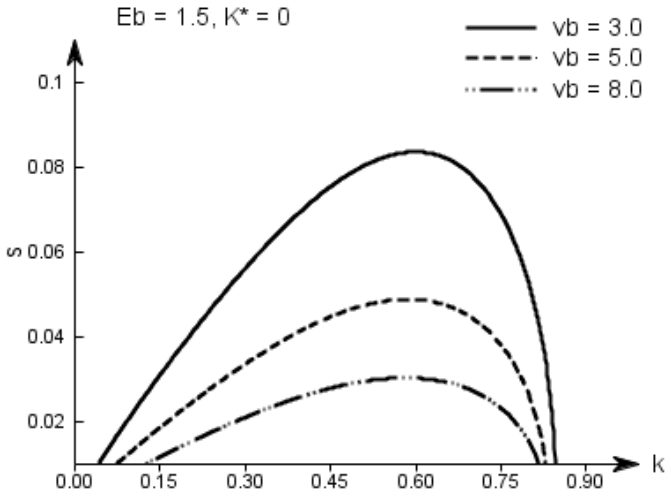

Figure 15. Positive real part of s as a function k with $K^* = 0, \nu^* = 0, \sigma_b = 0$, $E_b = 1.5$ and various v_b.

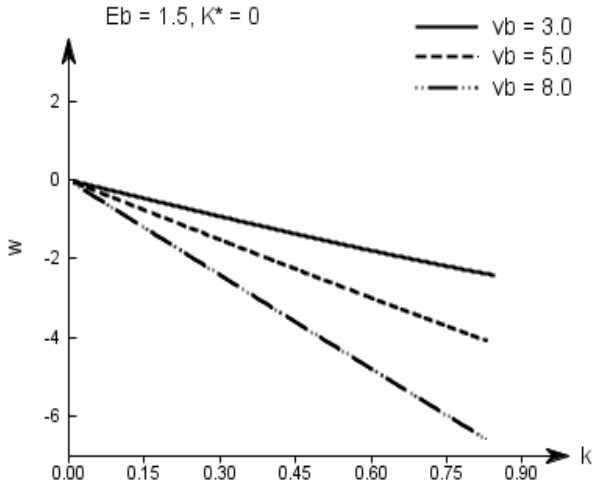

Figure 16. ω as a function k for various v_b with $K^* = 0, \nu^* = 0, \sigma_b = 0$ and $E_b = 1.5$.

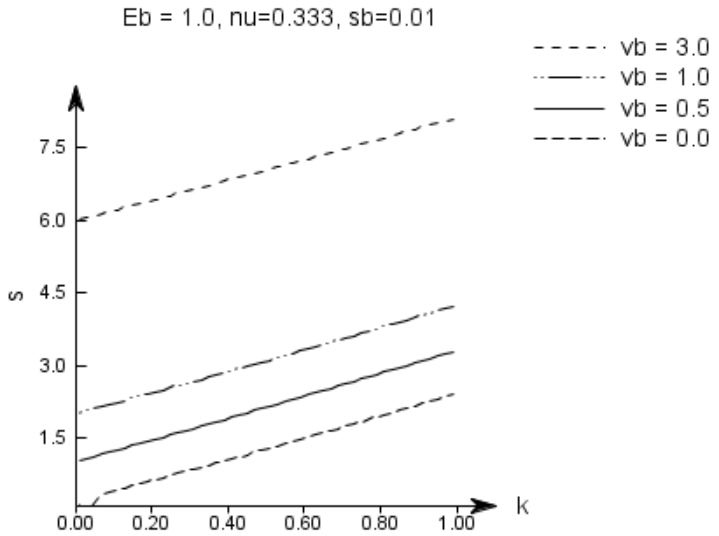

Figure 17. Positive real part of s as a function k with $K^* = \infty$, $E_b = 1.0, \nu^* = 0.333, \sigma_b = 0.01$ for various v_b.

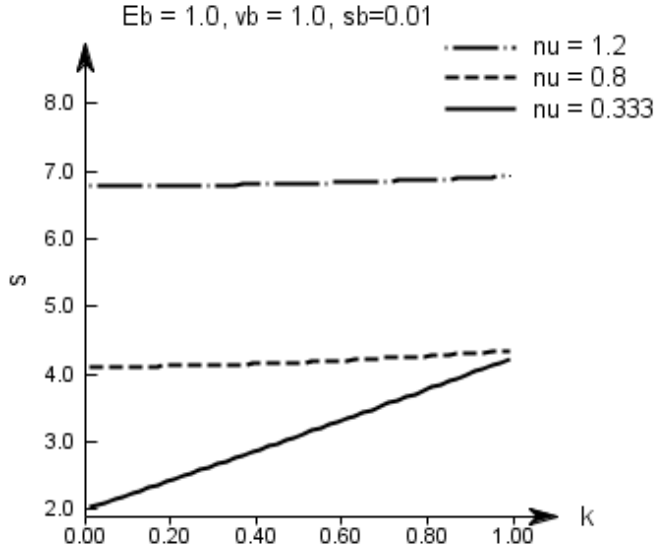

Figure 18. Positive real solutions of s as a function k with $\sigma_b = 0.01$, $E_b = 1.0$, $v_b = 1$ for various ν^* *and* $K^* = \infty$.

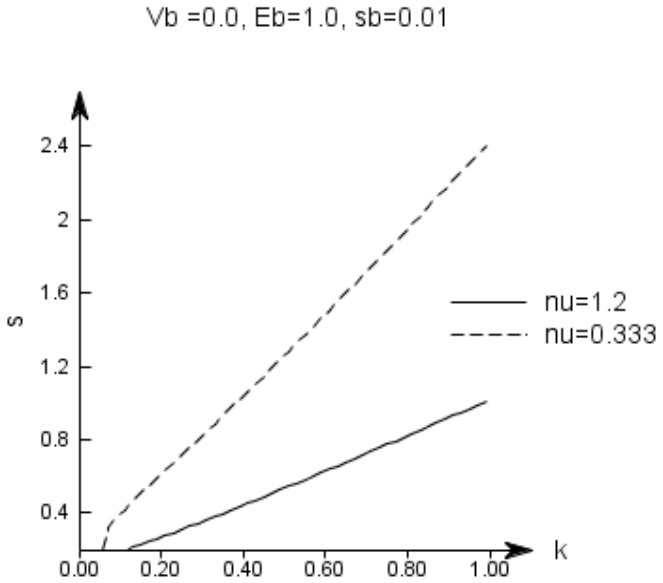

Figure 19. Positive real solutions of s as a function k with $K^* = \infty, \nu^* = 0.333\&1.2, E_b = 1.0$ and $\nu_b = 0$ for $\sigma_b = 0.01$

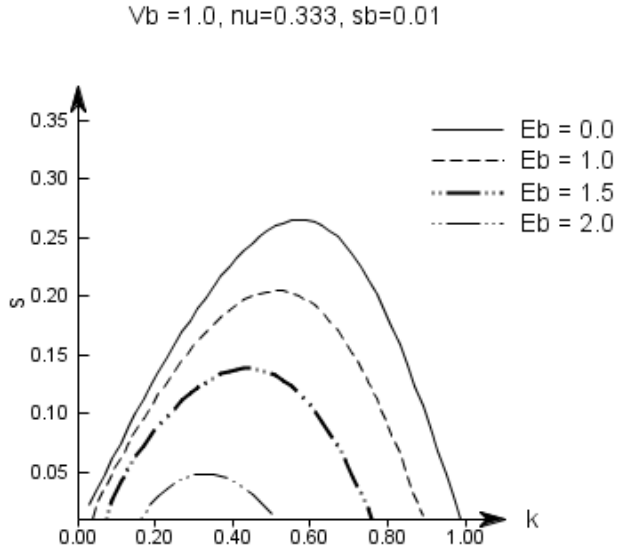

Figure 20. Secondary mode: positive real solutions of s as a function k with $K^* = \infty, \nu^* = 0.333, \sigma_b = 0.01$ and $\nu_b = 1$ for various E_b.

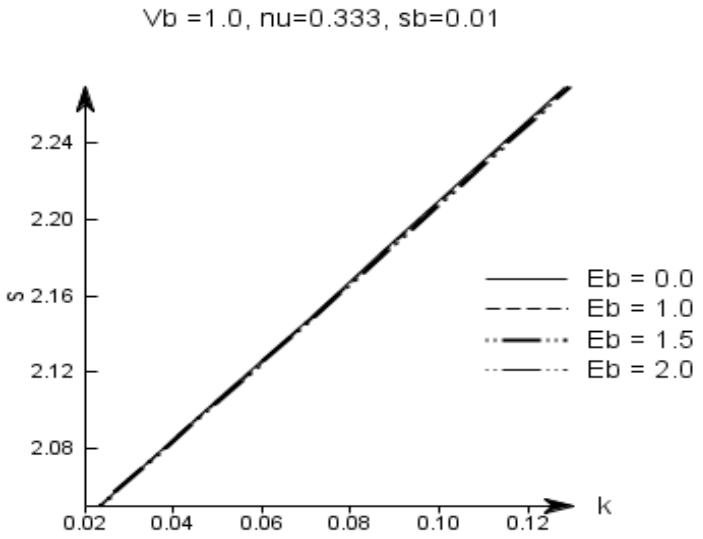

Figure 21. Primary mode: positive real solutions of s as a function *k* with $K^* = \infty, \nu^* = 0.333, \sigma_b = 0.01$ and $v_b = 1$ for various E_b.

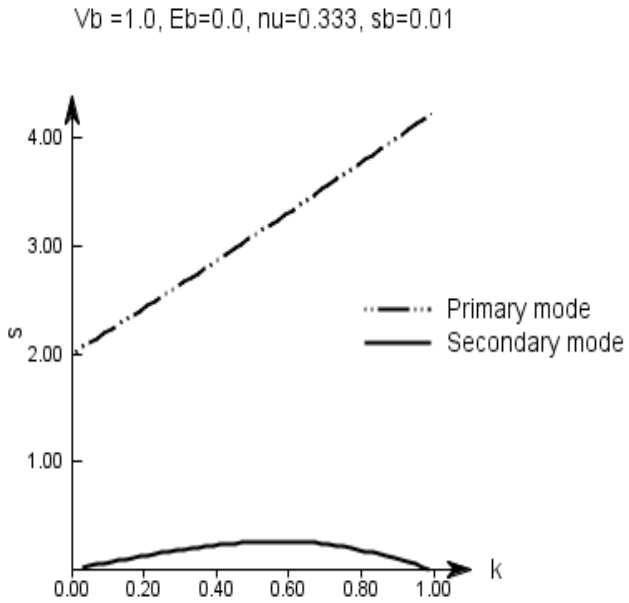

Figure 22. Primary and secondary modes with $K^* = \infty, \nu^* = 0.333, \sigma_b = 0.01,$ and $v_b = 1$ for $E_b = 0$

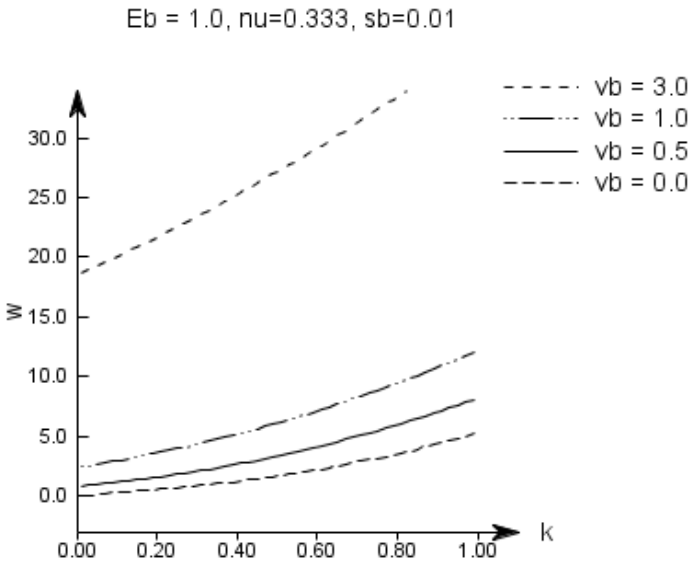

Figure 23. Real part of ω as a function of k with $K^* = \infty, \nu^* = 0.333, \sigma_b = 0.01, \ E_b = 1.0$ for various ν_b.

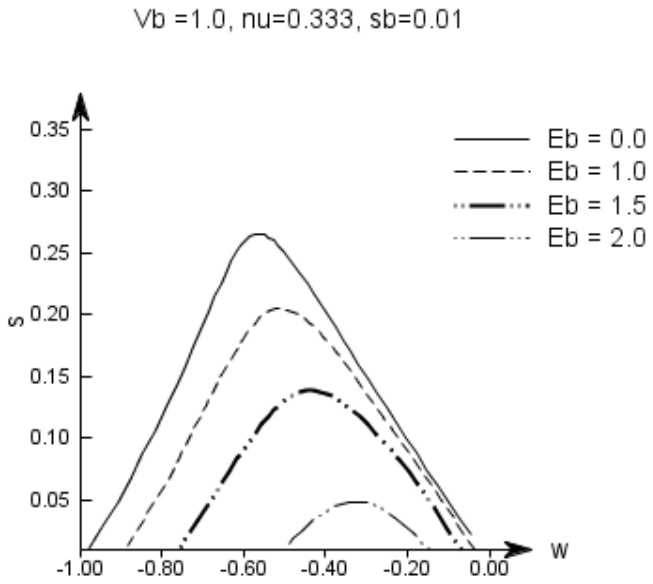

Figure 24. Growth rate s versus ω with $K^* = \infty, \nu^* = 0.333, \sigma_b = 0.01$ For various E_b.

2.7 Concluding Remarks

A dispersion relation for the problem of linear spatial instability of electrically driven viscous jets in the presence of an applied electric field and non-zero basic state velocity is derived. Two cases, namely, zero and infinite conductivity cases are considered. From our numerical results, we detected two modes of instability for the infinite conductivity jets. The instability modes were found to move along positive axial direction. The basic state velocity is found to be stabilizing for zero conductivity case, but destabilizing for infinite conductivity case. The most dangerous disturbances were found to be intrinsically viscous in nature only for the non-zero basic state velocity but in viscid for the zero value of the basic state velocity.

REFERENCES

- A. G. Baily. Electro-Static Spraying of Liquid, Wiley, New York, N.Y, (1981).
- M. M. Hohman, M. Shin, G. Rutledge and M. P. Brenner. Electrospinning and electrically forced jets. I. Stability theory, Physics of Fluids, 13(8) (2001a), 2201-2220.
- M. M. Hohman, M. Shin, G. Rutledge and M. P. Brenner. Electrospinning and electrically forced jets. II. Applications, Physics of Fluids, 13(8) (2001b), 2221-2236.
- P. G. Drazin and W.H. Reid. Hydrodynamic Stability, Cambridge University Press, UK, (1981).
- Saville D. A. (1971). Electrohydrodynamic stability: effects of charge relaxation at the interface of a liquid jet, J. Fluid Mech. **48**(4), 815-827.
- A. Michalke. On spatially growing disturbances in an in viscid shear layer, J. Fluid Mech. 23 (1965), 521-544.
- P. A. Monkewitz and P. Huerre. Influence of the velocity ratio on the spatial instability of mixing layers, Phys. Fluids, 25(7) (1982), 1137-1143.
- K. H. Lie and D.H. Riahi. Numerical solution of the Orr-Sommerfeld equation for mixing layers, Int. J. Eng. Sci. 26, (1988), 163-174.
- C. K. W. Tam and A. T. Thies.Instability of rectangular jets, J. Fluid Mech. 248 (1993), 425-448.

- D. L. Soderberg. Absolute and convective instability of a Relaxational plane liquid jet, J. Fluid Mech. 439 (2003), 89-119.
- J. J. Healey. In viscid axisymmetric absolute instability of swirling jets, J. Fluid Mech. 613 (2008), 1-33.
- D. H. Reneker, A. L. Yarin and H. Fong. Bending instability of electrically charged liquid jets of polymer solutions in electro spinning, J. Appl. Phys. 87 (2000), 4531-4547.
- V. Y. Shkadov and A. A. Shutov. Disintegration of a charged viscous jet in a high electric field, Fluid Dyn. Res. 28 (2001), 23-39.
- S. V. Fridrikh, J. H. Yu, M. P. Brenner and G.C. Rutledge .Controlling the fiber diameter during electrospinning, Phys. Rev. Lett., 90 (2003), 144502.
- D. Bhatta, S. Das, and D. N. Riahi. On temporal instability of electrically forced axisymmetric jets with variable applied field and nonzero basic state velocity, Applications and Applied Mathematics,(2010), accepted.
- Z. Sun, E. Zussman, A. L. Yarin, J. H. Wendorff and A. Greiner. Compound coreshell polymer nanofibers by co-electro spinning, Advanced Materials 15 (2003), 1929-1932.
- D. Li and Y. Xia. Direct fabrication of composite and ceramic hollow nanofibers by electrospinning, Nano. Lett. 4 (2004), 933-938.
- J. H. Yu, S. V. Fridrikh and G. C. Rutledge. Production of sub-micrometer diameter fibers by two-fluid electrospinning, Advanced Materials 16, (2004) 1562-1566.
- D. N. Riahi. On spatial instability of electrically forced axisymmetric jets with variable applied field, Appl. Math. Modeling, 33 (2009), 3546-3552.
- J. R. Melcher and G. I. Taylor. Electro-hydrodynamics: A review of the interfacial shear stresses, Annu. Rev. Fluid Mech. 1 (1969), 111-146.

- G. I. Taylor. Electrically driven jets, Proc. Royal Soc. A, 313 (1969), 453-475.

APPENDIX A

APPENDIX A

DETAILED COMPUTATIONAL PROCESS FOR TEMPORAL INSTABILTY

- ✓ We find the zeroes of the Dispersion Relation (DR), Equation (6), Pg 8.
- ✓ We solve the DR by using MATLAB Library function ROOTS
- ✓ ROOTS find all the zeroes of the complex equation. Its algorithm is based on calculating all the Eigen Values of the companion matrices
- ✓ We separate the real and imaginary part of the zeroes to get the growth rate (ω_r) and frequency (ω_i) of the system.
- ✓ We collected computational data for the figures based on the zero of the DR that give max growth rate ω_r , & for frequency plot we used the data for ω_i with various k (*)

(*) EXAMPLE OF MATRICES WE FORM AFTER SOLVING FOR ZEROES

k	ω_r	ω_i	ω_r	ω_i	ω_r	ω_i
0.01	(0.010047	-0.020431)	(-0.008594	-0.080702)	(-0.495019	-0.048867)
0.02	(0.016272	-0.066198)	(-0.016196	-0.134488)	(-1.615025	-0.099314)
0.03	(0.021657	-0.11303)	(-0.022321	-0.187501)	(-3.083021	-0.149469)
0.04	(0.026377	-0.1605)	(-0.027829	-0.239957)	(-4.710988	-0.199543)
0.05	(0.030628	-0.208443)	(-0.033015	-0.291975)	(-6.371063	-0.249583)
0.06	(0.034531	-0.256761)	(-0.038031	-0.343634)	(-7.982455	-0.299605)
0.07	(0.038168	-0.305385)	(-0.042966	-0.394997)	(-9.499135	-0.349617)
0.08	(0.04159	-0.354266)	(-0.047879	-0.446111)	(-10.898871	-0.399623)
0.09	(0.044834	-0.403362)	(-0.052807	-0.497014)	(-12.17464	-0.449624)

0.10	(0.047924	-0.452643)	(-0.057778	-0.547735)	(-13.328485	-0.499623)
0.11	(0.050878	-0.502081)	(-0.062809	-0.5983)	(-14.367406	-0.549619)
0.12	(0.053709	-0.551654)	(-0.067913	-0.648732)	(-15.300767	-0.599614)
0.13	(0.056424	-0.601345)	(-0.073098	-0.699047)	(-16.138716	-0.649608)
0.14	(0.059029	-0.651137)	(-0.078371	-0.749262)	(-16.891289	-0.699601)
0.15	(0.061527	-0.701016)	(-0.083734	-0.799391)	(-17.56793	-0.749593)
0.16	(0.063919	-0.750971)	(-0.089188	-0.849444)	(-18.177268	-0.799585)
0.17	(0.066205	-0.800993)	(-0.094735	-0.899431)	(-18.727046	-0.849577)
0.18	(0.068386	-0.851071)	(-0.100373	-0.949361)	(-19.224132	-0.899568)
0.19	(0.070458	-0.9012)	(-0.106101	-0.999241)	(-19.674571	-0.94956)
0.20	(0.07242	-0.951372)	(-0.111916	-1.049077)	(-20.083665	-0.999551)
0.21	(0.07427	-1.001583)	(-0.117816	-1.098874)	(-20.456051	-1.049543)
0.22	(0.076004	-1.051829)	(-0.123799	-1.148637)	(-20.795781	-1.099534)
0.23	(0.07762	-1.102105)	(-0.129861	-1.198368)	(-21.106394	-1.149526)
0.24	(0.079114	-1.152409)	(-0.136	-1.248073)	(-21.390986	-1.199518)
0.25	(0.080484	-1.202738)	(-0.142211	-1.297751)	(-21.652267	-1.249511)
0.26	(0.081725	-1.25309)	(-0.148492	-1.347407)	(-21.892612	-1.299503)
0.27	(0.082836	-1.303463)	(-0.15484	-1.397041)	(-22.114107	-1.349496)
0.28	(0.083812	-1.353856)	(-0.161251	-1.446654)	(-22.31859	-1.39949)
0.29	(0.08465	-1.404269)	(-0.167722	-1.496248)	(-22.50768	-1.449483)
0.30	(0.085347	-1.454699)	(-0.174249	-1.545823)	(-22.682806	-1.499478)
0.31	(0.085899	-1.505148)	(-0.18083	-1.59538)	(-22.845237	-1.549472)
0.32	(0.086304	-1.555615)	(-0.187461	-1.644918)	(-22.996097	-1.599467)
0.33	(0.086558	-1.606099)	(-0.194138	-1.694438)	(-23.136385	-1.649463)
0.34	(0.086657	-1.656601)	(-0.200858	-1.74394)	(-23.266993	-1.699459)
0.35	(0.086598	-1.707122)	(-0.207618	-1.793423)	(-23.388716	-1.749456)
0.36	(0.086379	-1.757661)	(-0.214415	-1.842886)	(-23.502266	-1.799453)
0.37	(0.085994	-1.80822)	(-0.221245	-1.892329)	(-23.608281	-1.849451)
0.38	(0.085442	-1.858799)	(-0.228105	-1.941751)	(-23.707332	-1.89945)
0.39	(0.084719	-1.9094)	(-0.234991	-1.991151)	(-23.799936	-1.949449)
0.40	(0.083821	-1.960023)	(-0.2419	-2.040528)	(-23.886555	-1.999449)
0.41	(0.082745	-2.01067)	(-0.248829	-2.08988)	(-23.967608	-2.04945)
0.42	(0.081486	-2.061342)	(-0.255773	-2.139206)	(-24.043472	-2.099452)
0.43	(-0.262728	-2.188505)	(0.080042	-2.112041)	(-24.114489	-2.149454)
0.44	(-0.269692	-2.237773)	(0.078409	-2.162769)	(-24.180967	-2.199458)
0.45	(-0.276661	-2.287011)	(0.076582	-2.213527)	(-24.243186	-2.249462)
0.46	(-0.283629	-2.336214)	(0.074558	-2.264318)	(-24.3014	-2.299468)
0.47	(-0.290593	-2.385381)	(0.072333	-2.315145)	(-24.355837	-2.349474)
0.48	(-0.29755	-2.434509)	(0.069902	-2.366009)	(-24.406706	-2.399482)
0.49	(-0.304494	-2.483595)	(0.067262	-2.416915)	(-24.454195	-2.449491)
0.50	(-0.31142	-2.532635)	(0.064406	-2.467864)	(-24.498475	-2.499501)
0.51	(-0.318325	-2.581626)	(0.061332	-2.518862)	(-24.539701	-2.549512)
0.52	(-0.325204	-2.630564)	(0.058034	-2.569911)	(-24.578011	-2.599525)
0.53	(-0.33205	-2.679445)	(0.054506	-2.621017)	(-24.613532	-2.649539)
0.54	(-0.33886	-2.728263)	(0.050745	-2.672183)	(-24.646376	-2.699554)
0.55	(-0.345627	-2.777013)	(0.046744	-2.723416)	(-24.676644	-2.749571)
0.56	(-0.352347	-2.825689)	(0.042497	-2.774721)	(-24.704426	-2.79959)
0.57	(-0.359012	-2.874284)	(0.038	-2.826106)	(-24.729802	-2.849611)
0.58	(-0.365617	-2.92279)	(0.033245	-2.877576)	(-24.75284	-2.899633)
0.59	(-0.372155	-2.9712)	(0.028226	-2.929142)	(-24.773601	-2.949658)
0.60	(-0.378621	-3.019504)	(0.022938	-2.980812)	(-24.792136	-2.999684)
0.61	(-0.385006	-3.067691)	(0.017372	-3.032596)	(-24.808488	-3.049713)
0.62	(-0.391304	-3.115749)	(0.011523	-3.084507)	(-24.82269	-3.099745)
0.63	(-0.397509	-3.163664)	(0.005383	-3.136558)	(-24.834768	-3.149778)

0.64	(-0.403612 -3.211421)	(-0.001055 -3.188764)	(-24.844739 -3.199815)
0.65	(-0.409607 -3.259003)	(-0.007797 -3.241142)	(-24.852612 -3.249854)
0.66	(-0.415488 -3.30639)	(-0.014852 -3.293713)	(-24.858388 -3.299897)
0.67	(-0.421246 -3.353558)	(-0.022224 -3.346499)	(-24.86206 -3.349943)
0.68	(-0.426878 -3.400483)	(-0.029919 -3.399525)	(-24.863611 -3.399992)
0.69	(-0.432379 -3.447133)	(-0.037942 -3.452822)	(-24.863015 -3.450046)
0.70	(-0.437746 -3.493475)	(-0.046295 -3.506422)	(-24.860238 -3.500103)
0.71	(-0.44298 -3.53947)	(-0.054976 -3.560365)	(-24.855235 -3.550165)
0.72	(-0.448087 -3.585074)	(-0.063981 -3.614695)	(-24.847949 -3.600231)
0.73	(-0.453076 -3.630237)	(-0.0733 -3.66946)	(-24.838315 -3.650303)
0.74	(-0.457966 -3.674902)	(-0.082913 -3.724717)	(-24.826251 -3.70038)
0.75	(-0.462787 -3.719011)	(-0.092791 -3.780525)	(-24.811666 -3.750464)
0.76	(-0.46758 -3.7625)	(-0.102891 -3.836946)	(-24.79445 -3.800554)
0.77	(-0.472406 -3.805304)	(-0.113154 -3.894045)	(-24.774479 -3.850651)
0.78	(-0.477343 -3.847365)	(-0.1235 -3.951879)	(-24.75161 -3.900756)
0.79	(-0.482488 -3.888637)	(-0.133833 -4.010493)	(-24.725677 -3.95087)
0.80	(-0.487955 -3.929093)	(-0.144038 -4.069914)	(-24.696495 -4.000993)
0.81	(-0.493868 -3.968731)	(-0.153991 -4.130142)	(-24.663847 -4.051127)
0.82	(-0.500348 -4.007583)	(-0.16357 -4.191145)	(-24.62749 -4.101272)
0.83	(-0.507503 -4.045704)	(-0.172666 -4.252866)	(-24.587144 -4.15143)
0.84	(-0.515418 -4.08317)	(-0.181196 -4.315227)	(-24.542488 -4.201603)
0.85	(-0.524148 -4.120061)	(-0.189101 -4.378148)	(-24.493155 -4.251791)
0.86	(-0.533727 -4.156453)	(-0.196349 -4.441549)	(-24.438722 -4.301998)
0.87	(-0.544165 -4.192406)	(-0.202928 -4.50537)	(-24.378703 -4.352224)
0.88	(-0.555466 -4.22796)	(-0.208834 -4.569566)	(-24.312534 -4.402474)
0.89	(-0.567627 -4.263134)	(-0.214067 -4.634116)	(-24.23956 -4.45275)
0.90	(-0.580654 -4.297927)	(-0.218621 -4.699017)	(-24.159014 -4.503056)
0.91	(-0.594556 -4.33232)	(-0.222485 -4.764284)	(-24.07 -4.553396)
0.92	(-0.609359 -4.366274)	(-0.225633 -4.829949)	(-23.971457 -4.603777)
0.93	(-0.625098 -4.399736)	(-0.228024 -4.896059)	(-23.862125 -4.654205)
0.94	(-0.641831 -4.432633)	(-0.2296 -4.962679)	(-23.740497 -4.704688)
0.95	(-0.659631 -4.464873)	(-0.230283 -5.02989)	(-23.604757 -4.755237)
0.96	(-0.678599 -4.496338)	(-0.229969 -5.097795)	(-23.452692 -4.805866)
0.97	(-0.698862 -4.526885)	(-0.228524 -5.166523)	(-23.281585 -4.856592)
0.98	(-0.720586 -4.556329)	(-0.225775 -5.236233)	(-23.088063 -4.907438)
0.99	(-0.743984 -4.584438)	(-0.2215 -5.307128)	(-22.867883 -4.958434)

Here ω_r--temporal growth rates and ω_i –frequency for given k-axial wave number.
For corresponding values of V_b=5, Conductivity of 19.3, v^*=0.33 and E_b=1.93, with σ=0.01

APPENDIX B

APPENDIX B

DETAILED COMPUTATIONAL PROCESS FOR SPATIAL INSTABILTY

We find the zeroes of the Dispersion Relation (DR) by following steps

- First while deriving the dispersion relation we separate the Real and Imaginary part of the dispersion relation by expanding the equation to the simplest form(*)
- We get two separate equations, where we have two unknown's, s (growth rate) and ω (frequency), with varying k (wavenumber).
- The important part is to get the right guess in order to follow the Iterative method to calculate the actual zeroes.
- We program to carry out findings of the initial guess in MATHEMATICA using NSOLVE (an inbuilt MATHEMATICA library function)(**)
- Using the initial guess we use Iterative method to carry out finding the actual zeroes. (***)
- We use this data to plot the figures

(*)THE DR AFTER EXPANDING THE IMAG & REAL PART TO ITS SIMPLEST FORM

Imaginary Part of DISPERSION RELATION:

$$-2\,[(E_b^2\,k^2\,K^*)/\sqrt{\beta}]+2\,\pi\,[\sqrt{\beta}\,k^4\,K^*\,L]-[\sqrt{\beta}\,E_b^{\,2}\,k^4\,K^*\,L]-2\,\pi\,[\sqrt{\beta}\,k^6\,K^*\,L]+2\,[(E_b^{\,2}\,K^*\,s^2)/\sqrt{\beta}]-12\,\pi\,[\sqrt{\beta}\,k^2\,K^*\,L\,s^2]+6\,[\sqrt{\beta}\,E_b^{\,2}\,k^2\,K^*\,L\,s^2]+30\,\pi\,[\sqrt{\beta}\,k^4\,K^*\,L\,s^2]+2\,\pi\,[\sqrt{\beta}\,K^*\,L\,s^4]-[\sqrt{\beta}\,E_b^{\,2}\,K^*\,L\,s^4]-30\,\pi\,[\sqrt{\beta}k^2\,K^*\,L\,s^4]+2\,\pi\,[\sqrt{\beta}\,K^*\,L\,s^6]-2\,[(E_b^{\,2}\,k^2\,\sigma)/\sqrt{\beta}]-2\,[\sqrt{\beta}\,E_b^{\,2}\,k^4\,L\,\sigma]-24\,\pi\,[E_b^2\,k^2\,K^*\,s\,\sigma]+48\,\pi\,[E_b^2\,k^2\,K^*\,L\,s\,\sigma]+2\,[(E_b^2\,s^2\,\sigma)/\sqrt{\beta}]+12\,[\sqrt{\beta}\,E_b^2\,k^2\,L\,s^2\,\sigma]+8\,\pi\,[E_b\,K^*\,s^3\,\sigma]-16\,\pi\,[E_b\,K^*\,L\,s^3\,\sigma]-2\,[\sqrt{\beta}\,E_b^{\,2}\,L\,s^4\,\sigma]-16\,\pi^2\,[\sqrt{\beta}\,k^4\,K^*\,L\,\sigma^2]-24\,\pi\,[E_b\,k^2\,s\,\sigma^2]+24\,\pi\,[E_b\,k^2\,L\,s\,\sigma^2]-20\,\pi\,[\beta\,E_b\,k^4\,L\,s\,\sigma^2]+96\,\pi 2\,[\sqrt{\beta}\,k^2\,K^*\,L\,s^2\,\sigma^2]+8\,\pi\,[E_b\,s^3\,\sigma^2]-8\,\pi\,[E_b\,L\,s^3\,\sigma^2]+40\,\pi\,[\beta\,E_b\,k^2\,L\,s^3\,\sigma^2]-16\,\pi 2\,[\sqrt{\beta}\,K^*\,L\,s^4\,\sigma^2]-4\,\pi\,[\beta\,E_b\,L\,s^5\,\sigma^2]+3\,[k^2\,s\,v_b]-5\,[k^4\,s\,v_b]+(5/2)\,[\beta\,k^4\,L\,s\,v_b]-5\,[\beta\,E_b^{\,2}\,k^4\,L\,s\,v_b]/(4\,\pi)-(7/2)\,[\beta\,k^6\,L\,s\,v_b]-[s^3\,v_b]+10\,[k^2\,s^3\,v_b]-5\,[\beta\,k^2\,L\,s^3\,v_b]+5\,[\beta\,E_b^{\,2}\,k^2\,L\,s^3\,v_b]/(2\,\pi)+(35/2)\,[\beta\,k^4\,L\,s^3\,v_b]-[s^5\,v_b]+(1/2)\,[\beta\,L\,s^5\,v_b]-[\beta\,E_b^{\,2}\,L\,s^5\,v_b]/(4\,\pi)-(21/2)\,[\beta\,k^2\,L\,s^5\,v_b]+(1/2)\,[\beta\,L\,s^7\,v_b]+2\,[(E_b\,k^2\,\sigma\,v_b)/\,\mathrm{sqrt}\beta]+2\,[\sqrt{\beta}\,E_b\,k^4\,L\,\sigma\,v_b]-2\,[(E_b\,s^2\,\sigma\,v_b)/\sqrt{\beta}]-12\,[\sqrt{\beta}\,E_b\,k^2\,L\,s^2\,\sigma\,v_b]+2\,[\sqrt{\beta}\,E_b\,L\,s^4\,\sigma\,v_b]+48\,\pi\,[k^2\,s\,\sigma^2\,v_b]-72\,\pi\,[k^2\,L\,s\,\sigma^2\,v_b]+40\,\pi\,[\beta\,k^4\,L\,s\,\sigma^2\,v_b]-16\,\pi\,[s^3\,\sigma^2\,v_b]+24\,\pi\,[L\,s^3\,\sigma^2\,v_b]-80\,\pi\,[\beta\,k^2\,L\,s^3\,\sigma^2\,v_b]+8\,\pi\,[\beta\,L\,s^5\,\sigma^2\,v_b]-60\,\pi\,[\sqrt{\beta}\,k^4\,K^*\,L\,s\,v^*\,v_b]+120\,\pi\,[\sqrt{\beta}\,k^2\,K^*\,L\,s^3\,v^*\,v_b]-12\,\pi\,[\sqrt{\beta}\,K^*\,L\,s^5$$

$v^* v_b]+4\ \pi\ [\sqrt{\boldsymbol{\beta}}\ k^4\ K^*\ L\ v_b{}^2]-24\ \pi\ [\sqrt{\boldsymbol{\beta}}\ k^2\ K^*\ L\ s^2\ v_b{}^2]+4\ \pi\ [\sqrt{\boldsymbol{\beta}}\ K^*\ L\ s^4\ v_b{}^2]+6\ [k^4\ v^*\ v_b{}^2]+3\ [\beta\ k^6\ L\ v^*\ v_b{}^2]-36\ [k^2\ s^2\ v^*\ v_b{}^2]-45\ [\beta\ k^4\ L\ s^2\ v^*\ v_b{}^2]+6\ [s^4\ v^*\ v_b{}^2]+45\ [\beta\ k^2\ L\ s^4\ v^*\ v_b{}^2]-3\ [\beta\ L\ s^6\ v^*\ v_b{}^2]+6\ [k^2\ s\ v_b{}^3]+5\ [\beta\ k^4\ L\ s\ v_b{}^3]-2\ [s^3\ v_b{}^3]-10\ [\beta\ k^2\ L\ s^3\ v_b{}^3]+[\beta\ L\ s^5\ v_b{}^3]+2\ [k\ s\ \omega]-4\ [k^3\ s\ \omega]+2\ [\beta\ k^3\ L\ s\ \omega]-[\beta\ E_b{}^2\ k^3\ L\ s\ \omega]/\pi-3\ [\beta\ k^5\ L\ s\ \omega]+4\ [k\ s^3\ \omega]-2\ [\beta\ k\ L\ s^3\ \omega]+[\beta\ E_b{}^2\ k\ L\ s^3\ \omega]/\pi+10\ [\beta\ k^3\ L\ s^3\ \omega]-3\ [\beta\ k\ L\ s^5\ \omega]+16\ \pi\ [k\ s\ \sigma^2\ \omega]-32\ \pi\ [k\ L\ s\ \sigma^2\ \omega]+16\ \pi\ [\beta\ k^3\ L\ s\ \sigma^2\ \omega]-16\ \pi\ [\beta\ k\ L\ s^3\ \sigma^2\ \omega]-48\ \pi\ [\sqrt{\boldsymbol{\beta}}\ k^3\ K^*\ L\ s\ v^*\ \omega]+48\ \pi\ [\sqrt{\boldsymbol{\beta}}\ k\ K^*\ L\ s^3\ v^*\ \omega]+8\ \pi\ [\sqrt{\boldsymbol{\beta}}\ k^3\ K^*\ L\ v_b\ \omega]-24\ \pi\ [\sqrt{\boldsymbol{\beta}}\ k\ K^*\ L\ s^2\ v_b\ \omega]+12\ [k^3\ v^*\ v_b\ \omega]+6\ [\beta\ k^5\ L\ v^*\ v_b\ \omega]-36\ [k\ s^2\ v^*\ v_b\ \omega]-60\ [\beta\ k^3\ L\ s^2\ v^*\ v_b\ \omega]+30\ [\beta\ k\ L\ s^4\ v^*\ v_b\ \omega]+12\ [k\ s\ v_b{}^2\ \omega]+12\ [\beta\ k^3\ L\ s\ v_b{}^2\ \omega]-12\ [\beta\ k\ L\ s^3\ v_b{}^2\ \omega]+4\ \pi\ [\sqrt{\boldsymbol{\beta}}\ k^2\ K^*\ L\ \omega^2]-4\ \pi\ [\sqrt{\boldsymbol{\beta}}\ K^*\ L\ s^2\ \omega^2]+6\ [k^2\ v^*\ \omega^2]+3\ [\beta\ k^4\ L\ v^*\ \omega^2]-6\ [s^2\ v^*\ \omega^2]-18\ [\beta\ k^2\ L\ s^2\ v^*\ \omega^2]+3\ [\beta\ L\ s^4\ v^*\ \omega^2]+6\ [s\ v_b\ \omega^2]+9\ [\beta\ k^2\ L\ s\ v_b\ \omega^2]-3\ [\beta\ L\ s^3\ v_b\ \omega^2]+2\ [\beta\ k\ L\ s\ \omega^3]$

Real part of DISPERSION RELATION:

$(4\ E_b{}^2\ k\ K^*\ s)/\sqrt{\beta}+4\sqrt{\beta}\ E_b{}^2\ k^3\ K^*\ L\ s-8\sqrt{\beta}\ k^3\ K^*\ L\ \pi\ s+12\sqrt{\beta}\ k^5\ K^*\ L\ \pi\ s-4\sqrt{\beta}\ E_b{}^2\ k\ K^*\ L\ s^3+8\sqrt{\beta}\ k\ K^*\ L\ \pi\ s^3-40\sqrt{\beta}\ k^3\ K^*\ L\ \pi\ s^3+12\sqrt{\beta}\ k\ K^*\ L\ \pi\ s^5-8\ E_b\ k^3\ K^*\ \pi\ \sigma+16\ E_b\ k^3\ K^*\ L\ \pi\ \sigma+(4\ E_b{}^2\ k\ s\ \sigma)/\sqrt{\beta}+8\sqrt{\beta}E_b{}^2\ k^3\ L\ s\ \sigma+24\ E_b\ k\ K^*\ \pi\ s^2\ \sigma-48\ E_b\ k\ K^*\ L\ \pi\ s^2\ \sigma-8$

$\sqrt{\beta}\ E_b^{\,2}\ k\ L\ s^3\ \sigma - 8\ E_b\ k^3\ \pi\ \sigma^2 + 8\ E_b\ k^3\ L\ \pi\ \sigma^2 - 4\ \beta\ E_b\ k^5\ L\ \pi\ \sigma^2 + 64\ \sqrt{\beta}\ k^3\ K^*\ L\ \pi 2\ s\ \sigma^2 + 24\ E_b\ k\ \pi\ s^2\ \sigma^2 - 24\ E_b\ k\ L\ \pi\ s^2\ \sigma^2 + 40\ \beta\ E_b\ k^3\ L\ \pi\ s^2\ \sigma^2 - 64\ \sqrt{\beta}\ k\ K^*\ L\ \pi 2\ s^3\ \sigma^2 - 20\ \beta\ E_b\ k\ L\ \pi\ s^4\ \sigma^2 + k^3\ v_b - k^5\ v_b + 1/2\ \beta\ k^5\ L\ v_b - 1/2\ \beta\ k^7\ L\ v_b - (\beta\ E_b^{\,2}\ k^5\ L\ v_b)/(4\ \pi) - 3\ k\ s^2\ v_b + 10\ k^3\ s^2\ v_b - 5\ \beta\ k^3\ L\ s^2\ v_b + 21/2\ \beta\ k^5\ L\ s^2\ v_b + (5\ \beta\ E_b^{\,2}\ k^3\ L\ s^2\ v_b)/(2\ \pi) - 5\ k\ s^4\ v_b + 5/2\ \beta\ k\ L\ s^4\ v_b - 35/2\ \beta\ k^3\ L\ s^4\ v_b - (5\ \beta\ E_b^{\,2}\ k\ L\ s^4\ v_b)/(4\ \pi) + 7/2\ \beta\ k\ L\ s^6\ v_b - (4\ E_b\ k\ s\ \sigma\ v_b)/\sqrt{\beta} - 8\ \sqrt{\beta}\ E_b\ k^3\ L\ s\ \sigma\ v_b + 8\ \sqrt{\beta}\ E_b\ k\ L\ s^3\ \sigma\ v_b + 16\ k^3\ \pi\ \sigma^2\ v_b - 24\ k^3\ L\ \pi\ \sigma^2\ v_b + 8\ \beta\ k^5\ L\ \pi\ \sigma^2\ v_b - 48\ k\ \pi\ s^2\ \sigma^2\ v_b + 72\ k\ L\ \pi\ s^2\ \sigma^2\ v_b - 80\ \beta\ k^3\ L\ \pi\ s^2\ \sigma^2\ v_b + 40\ \beta\ k\ L\ \pi\ s^4\ \sigma^2\ v_b - 12\ \sqrt{\beta}\ k^5\ K^*\ L\ \pi\ v^*\ v_b + 120\ \sqrt{\beta}\ k^3\ K^*\ L\ \pi\ s^2\ v^*\ v_b - 60\ \sqrt{\beta}\ k\ K^*\ L\ \pi\ s^4\ v^*\ v_b - 16\ \sqrt{\beta}\ k^3\ K^*\ L\ \pi\ s\ v_b^{\,2} + 16\ \sqrt{\beta}\ k\ K^*\ L\ \pi\ s^3\ v_b^{\,2} - 24\ k^3\ s\ v^*\ v_b^{\,2} - 18\ \beta\ k^5\ L\ s\ v^*\ v_b^{\,2} + 24\ k\ s^3\ v^*\ v_b^{\,2} + 60\ \beta\ k^3\ L\ s^3\ v^*\ v_b^{\,2} - 18\ \beta\ k\ L\ s^5\ v^*\ v_b^{\,2} + 2\ k^3\ v_b^{\,3} + \beta\ k^5\ L\ v_b^3 - 6\ k\ s^2\ v_b^{\,3} - 10\ \beta\ k^3\ L\ s^2\ v_b^{\,3} + 5\ \beta\ k\ L\ s^4\ v_b^{\,3} + k^2\ \omega - k^4\ \omega + 1/2\ \beta\ k^4\ L\ \omega - 1/2\ \beta\ k^6\ L\ \omega - (\beta\ E_b^{\,2}\ k^4\ L\ \omega)/(4\ \pi) - s^2\ \omega + 6\ k^2\ s^2\ \omega - 3\ \beta\ k^2\ L\ s^2\ \omega + 15/2\ \beta\ k^4\ L\ s^2\ \omega + (3\ \beta\ E_b^{\,2}\ k^2\ L\ s^2\ \omega)/(2\ \pi) - s^4\ \omega + 1/2\ \beta\ L\ s^4\ \omega - 15/2\ \beta\ k^2\ L\ s^4\ \omega - (\beta\ E_b^{\,2}\ L\ s^4\ \omega)/(4\ \pi) + 1/2\ \beta\ L\ s^6\ \omega + 8\ k^2\ \pi\ \sigma^2\ \omega - 16\ k^2\ L\ \pi\ \sigma^2\ \omega + 4\ \beta\ k^4\ L\ \pi\ \sigma^2\ \omega - 8\ \pi\ s^2\ \sigma^2\ \omega + 16\ L\ \pi\ s^2\ \sigma^2\ \omega - 24\ \beta\ k^2\ L\ \pi\ s^2\ \sigma^2\ \omega + 4\ \beta\ L\ \pi\ s^4\ \sigma^2\ \omega - 12\ \sqrt{\beta}\ k^4\ K^*\ L\ \pi\ v^*\ \omega + 72\ \sqrt{\beta}\ k^2\ K^*\ L\ \pi\ s^2\ v^*\ \omega - 12\ \sqrt{\beta}\ K^*\ L\ \pi\ s^4\ v^*\ \omega - 24\ \sqrt{\beta}\ k^2\ K^*\ L\ \pi\ s\ v_b\ \omega + 8\ \sqrt{\beta}\ K^*\ L\ \pi\ s^3\ v_b\ \omega - 36\ k^2\ s\ v^*\ v_b\ \omega - 30\ \beta\ k^4\ L\ s\ v^*\ v_b\ \omega + 12\ s^3\ v^*\ v_b\ \omega + 60\ \beta\ k^2\ L\ s^3\ v^*\ v_b\ \omega - 6\ \beta\ L\ s^5\ v^*\ v_b\ \omega + 6\ k^2\ v_b^{\,2}\ \omega + 3\ \beta\ k^4\ L\ v_b^{\,2}\ \omega - 6\ s^2\ v_b^{\,2}\ \omega - 18\ \beta\ k^2\ L\ s^2\ v_b^{\,2}\ \omega + 3\ \beta\ L\ s^4\ v_b^{\,2}\ \omega - 8\ \sqrt{\beta}\ k$

K* L π s ω^2-12 k s v* ω^2-12 β k^3 L s v* ω^2+12 β k L s^3 v* ω^2+6 k v_b ω^2+3 β k^3 L v_b ω^2-9 β k L s^2 v_b ω^2+2 ω^3+β k^2 L ω^3-β L s^2 ω

(**) AN EXAMPLE OF INTIAL GUESS FINDING USING MATHEMATICA

Below is an example of finding the real values of max(s) and corresponding (ω), which we use in finding the respective zeroes by using Iterative Method to solve the two(Real and Imaginary) equations with two unknowns s and ω.

Zero Conductivity case with k = 0.03E_b= 2, v_b = 0.1, v=0, σ=0.*

{{{s→0. -0.708508 i,ω→-0.0738508},{s→0. +0.708508 i, ω→-0.0738508}, {s→0. -0.642751 i, ω→0.0666735},{s→0. +0.642751 i, ω→0.0666735}, {s→0. -0.638146 i, ω→0.0608146},{s→0. +0.638146 i,ω→0.0608146},{**s→0.194618,ω→-0.0733889**},{s→-0.0979184-0.0411591 i,ω→0.029127 +0.0612244 i},{s→-0.0979184+0.0411591 i,ω→0.029127 -0.0612244 i},{s→0.0739401 -0.0631433 i,ω→-0.0377694+0.0491172 i},{s→0.0739401 +0.0631433 i,ω→-0.0377694-0.0491172 i},{s→0.130908 -0.0270205 i,ω→-0.00570205-0.0130908 i},{s→0.130908 +0.0270205 i,ω→-0.00570205+0.0130908 i},{s→-0.130908-0.0270205 i,ω→-0.00570205+0.0130908 i},{s→-0.130908+0.0270205 i,ω→-0.00570205-0.0130908 i},{s→-0.194618,ω→-0.0733889},{s→0.0979184 +0.0411591 i,ω→0.029127 +0.0612244 i},{s→0.0979184 -0.0411591 i,ω→0.029127 -0.0612244 i},{s→0.00784607 -0.0277988 i,ω→-0.00577988-0.000784607 i},{s→0.00784607 +0.0277988 i,ω→-0.00577988+0.000784607 i},{s→-0.00784607-0.0277988 i,ω→-0.00577988+0.000784607 i},{s→-

0.00784607+0.0277988 𝕚,ω→-0.00577988-0.000784607 𝕚},{s→-0.0739401+0.0631433 𝕚,ω→-0.0377694+0.0491172 𝕚},{s→-0.0739401-0.0631433 𝕚,ω→-0.0377694-0.0491172 𝕚}}}

Given above is a particular case of zero conductivity case, similarly we use for infinite conductivity cases and various other parameters.

In this particular case, we found out the max of Real s, in BOLD.

Here 𝕚 is the imaginary unit

NOTE: Other values that this example shows are the possible imaginary zeroes of the two equations, we solved, which we ignore for our case.

(***)AN EXAMPLE OF A MATRIX WE GET AFTER SOLVING THE EQUATIONS BY ITERATIVE METHOD

k	s	w
0.010	6.026066111114	18.520672978476
0.030	6.066284556886	18.825374998796
0.050	6.106631867229	19.133683186524
0.070	6.147105508764	19.445613793353
0.090	6.187702991798	19.761176366428
0.110	6.228421874667	20.080378922421
0.130	6.269259764377	20.403228792190
0.150	6.310214316418	20.729732878688
0.170	6.351283234286	21.059897763029
0.190	6.392464268869	21.393729757665
0.210	6.433755217761	21.731234937402
0.230	6.475153924537	22.072419159857
0.250	6.516658277991	22.417288080369
0.270	6.558266211370	22.765847163730
0.290	6.599975701577	23.118101694003
0.310	6.641784768381	23.474056783089
0.330	6.683691473609	23.833717378457
0.350	6.725693920336	24.197088270279
0.370	6.767790252077	24.564174098136
0.390	6.809978651966	24.934979357408

0.410	6.852257341944	25.309508405422
0.430	6.894624581941	25.687765467445
0.450	6.937078669051	26.069754642557
0.470	6.979617936713	26.455479909476
0.490	7.022240753885	26.844945132391
0.510	7.064945524208	27.238154066854
0.530	7.107730685172	27.635110365819
0.550	7.150594707257	28.035817585909
0.570	7.193536093075	28.440279194006
0.590	7.236553376470	28.848498574333
0.610	7.279645121605	29.260479036160
0.630	7.322809921995	29.676223822403
0.650	7.366046399484	30.095736119390
0.670	7.409353203149	30.519019068223
0.690	7.452729008088	30.946075778280
0.710	7.496172514066	31.376909343628
0.730	7.539682443953	31.811522863436
0.750	7.583257541881	32.249919467918
0.770	7.626896570987	32.692102352053
0.790	7.670598310596	33.138074820373
0.810	7.714361552544	33.587840347836
0.830	7.758185096272	34.041402664464
0.850	7.802067742018	34.498765875986
0.870	7.846008281070	34.959934640405
0.890	7.890005481317	35.424914434042
0.910	7.934058064986	35.893711965786
0.930	7.978164672928	36.366335846768
0.950	8.022323804592	36.842797721529
0.970	8.066533711504	37.323114281386
0.990	8.110792195555	37.807311084627

Here ω-frequency and s-spatial growth rates for given k-axial wave numer.
The pair ω and s correspond to values of v_b=3, of Infinite Conductivity, v^*=0.33, E_b=1.5 with σ=0.01

BIOGRAPHICAL SKETCH

Sayantan Das (SD). Was born in Kolkata, WB, India. He obtained his Bachelors in Electrical Engineering from Meghnad Saha institute of Technology, affiliated by West Bengal University of Technology, India in 2009.

Applying mathematics to real life and practical problems is what drove SD to complete his Master Degree. He had the opportunity to attend several summer research programs in very prestigious universities that included Wesleyan University, CT 2007-2008. He also had the opportunity to present his work at several conferences that included HUGHES 2007-2008, HESTEC 2010. He will start his PhD studies this upcoming fall 2011.

SD always welcomes comments and suggestions about his research work. The best way to get in touch with him is via email, i.e. sayan.polo@gmail.com ☺